Update to TJNAF E-03-109: Spin Asymmetries on the Nucleon Experiment - SANE

2006

J. Jourdan, M. Kotulla
University of Basel, Basel, Switzerland

L. Pentchev
College of William and Mary, Williamsburg, VA

W. Boeglin, S. Dhamija, P. Markowitz, J. Reinhold
Florida International University, Miami, FL

I. Albayrak, E. Christy, C. Keppel, V. Tvaskis
Hampton University, Hampton, VA

A. Vasiliev
Institute for High Energy Physics, Protvino, Moscow Region, Russia

M. Khandaker, F. Wesselmann
Norfolk State University, Norfolk, VA

A. Ahmidouch, S. Danagoulian
North Carolina A&M State University, Greensboro, NC

C. Butuceanu, G. Huber
University of Regina, Regina, SK

V. Kubarovsky
Rensselaer Polytechnic Institute, Troy, NY

R. Gilman, X. Jiang
Rutgers University, New Brunswick, NJ

S. Choi (cospokesperson), Ho-young Kang, Hyekoo Kang,
Byungwuek Lee, Yoomin Oh, Jeongseog Song
Seoul University, Seoul, Korea

Z.-E. Meziani (cospokesperson), B. Sawatzky
Temple University, Philadelphia, PA

P. Bosted, J.-P. Chen, V. Dharmawardarne, R. Ent, D. Gaskell, J. Gomez,
D. Higinbotham, M. Jones, D. Mack, J. Roche, G. Smith, B. Wojtsekhowski, S. Wood
Thomas Jefferson National Accelerator Facility, Newport News, VA

M. Bychkov, D. Crabb, M. Commisso, D. Day, E. Frlež, K. Kovacs, N. Liyanage,
J. Maxwell, D. Počanić, O. Rondon (cospokesperson), K. Slifer, S. Tajima
University of Virginia, Charlottesville, VA

A. Asaturyan, A. Mkrtchyan, H. Mkrtchyan, V. Tadevosyan
Yerevan Physics Institute, Yerevan, Armenia

Abstract

This document is an update on TJNAF E-03-109, the Spin Asymmetries on the Nucleon Experiment - SANE, conditionally approved in June 2003 by PAC24 for 27 days of beam in Hall C. Our collaboration has been working for the past three years preparing the detector elements, polarized target and auxiliary systems to be ready for installation and data taking in the first half of 2008. SANE is a measurement of the proton spin structure function g_2 and spin asymmetry A_1 over a broad range of the Bjorken scaling variable x from 0.3 to 0.8, for four-momentum transfers from 2.5 GeV^2 to 6.5 GeV^2. The experiment will measure inclusive double spin asymmetries using CEBAF polarized electron beams of about 4.8 and 6 GeV energies, scattered off the UVA solid polarized NH_3 target. The scattered electrons will be detected in the novel, large acceptance non-magnetic detector BETA (Big Electron Telescope Array), consisting of a forward tracking hodoscope (new in this update), a threshold Cherenkov detector, a Lucite tracking hodoscope and the BigCal electromagnetic calorimeter. Experimental asymmetries will be measured for the configurations of parallel beam and target spins, and target spin at 80° relative to the beam, from which we will obtain the physics spin asymmetries A_1 and A_2, and the spin structure functions, with minimal external input in the form of the unpolarized structure functions R and F_1. In this document we give only a brief review of the status of the proton transverse spin structure function, and concentrate on progress reports on the construction of BETA and related calibration plans, collaboration status and beam request. More extensive discussion of the physics motivation and details of the detector performance are given in the original proposal, which is part of this submission.

Contents

1 Brief Review of the Status of the Nucleon Spin Structure

After nearly 30 years of experimental and theoretical work, the study of the nucleon spin structure has entered a mature stage, reaching beyond the exploration of the properties of the polarized structure functions in the scaling regime into the region of the Bjorken scaling variable x near its unity upper limit. Moreover, the experimental techniques have expanded beyond the original simple approach of measuring DIS inclusive double spin asymmetries [1, 2, 3, 4, 5, 6] for parallel beam and target spins, or even for parallel and orthogonal configurations [7, 8, 9, 10, 11], to semi-inclusive measurements with detection of a π or K meson in coincidence with the scattered electron [12, 13] and the investigation of the gluon polarization [14, 15]. From the inclusive measurements in DIS it has been established that the quarks carry only about 25% of the nucleon spin, and from the inclusive and semi-inclusive measurements, the quark polarization by flavor has been determined [12, 16, 17].

The modern description of nucleon structure is done in terms of eight distributions functions, three of which are leading twist and independent of the quark transverse momentum $\vec{k}_\perp$ ($q(x)$, related to the unpolarized structure function (SF) F_1, $\Delta q(x)$, related to the spin SF g_1, and transversity $\delta(x)$ or $h_T(x)$), while the others involve both longitudinal and transverse components ($g_T = g_1 + g_2$, Collins $h_{1T}^\perp$, Sivers $f_{1T}^\perp$, $h_{1L}^\perp$ and $h_1^\perp$). Only F_1, g_1 and g_T can be investigated with inclusive measurements, all others require semi-inclusive experiments.

Inclusive measurements have obvious advantages over semi-inclusive ones in terms of simplicity of execution, and they can be used to further extend our understanding of the nucleon spin structure by focusing on the still poorly known transverse spin SF g_T. Moreover, the DIS process in the high x region is confined to high values of the four-momentum transfer squared $Q^2 = -q_\mu^2$, which experimentally is difficult to access, even in inclusive measurements. For this reason, precision studies of the nucleon spin structure in the high x region so far have concentrated on the spin structure of the nucleon resonances [18, 19, 16, 20, 21]. The precision exploration of DIS spin structure at high x has barely started with Jefferson Lab's Hall A measurement on the neutron [17, 22]. There are no comparable results for the proton, and no precision high-x results on g_T for either nucleon.

The mixed twist g_T measures the polarization of quarks with spins perpendicular to the virtual photon spin. It is related to the virtual Compton scattering spin asymmetry $A_2 = \sigma_{LT}/\sigma_T$, which is formed from the longitudinal-transverse interference cross section σ_{LT} and the transverse cross section σ_T. In terms of A_2, g_T can be expressed as $g_T = (\nu/\sqrt{Q^2})F_1 A_2$, where $\nu = E - E'$ represents the energy loss of a lepton with initial energy E. The leading twist-3 part of g_T comes from the corresponding twist-3 piece of g_2. The latter consists of a twist-2 part g_2^{WW}[23] and a mixed twist-2/twist-3 part $\overline{g}_2$ [24, 25]

$$\begin{aligned} g_2(x,Q^2) &= g_2^{WW}(x,Q^2) + \overline{g}_2(x,Q^2) \\ g_2^{WW}(x,Q^2) &= -g_1(x,Q^2) + \int_x^1 g_1(y,Q^2)\frac{dy}{y} \\ \overline{g}_2(x,Q^2) &= -\int_x^1 \frac{\partial}{\partial y}\Big(\frac{m}{M}h_T(y,Q^2)y + \xi(y,Q^2)\Big)\frac{dy}{y} \end{aligned} \tag{1}$$

where m and M are quark and nucleon masses, and $h_T(x,Q^2)$ is the chiral-odd quark transverse spin distribution. ξ represents a leading twist-3 contribution from processes involving quark-gluon interactions. In addition to g_2^{WW}, g_2 gets another twist-2 contribution from the transversity h_T, although in DIS this contribution is suppressed by the ratio m/M[26, 24, 25]. With this suppression of h_T, the third moment of the mixed twist $\overline{g}_2(x,Q^2)$ can be related by the operator product

expansion (OPE) to the reduced twist-3 quark matrix element d_2

$$\int_0^1 x^2 \overline{g}_2(x,Q^2)dx = \frac{1}{3}d_2(Q^2), \tag{2}$$

which can be calculated in lattice QCD [27]. However, it should be kept in mind that since h_T is a leading twist quantity (and therefore comparable in magnitude to g_1,) even if the ratio m/M were of the order of $\sim 1\%$, h_T could represent a significant contribution to $\overline{g}_2$, since the pure twist-3 piece ξ may be considerably smaller than g_1.

Only a handful of measurements of d_2 exist, from SLAC [7, 10, 11] and *RSS* [20] at Jefferson Lab. The SLAC measurements have been combined into a single number for the proton $d_2(Q^2 = 5\ \mathrm{GeV}^2) = 0.0032 \pm 0.0017$. The lattice QCD result at the same Q^2 is $d_2 = 0.004 \pm 0.005$. The *RSS* proton result covers a wide range of x from 0.29 to 0.84, corresponding to the region of the resonances from $W = 1.91$ GeV to the pion production threshold. The measured $\overline{d}_2(Q^2 = 1.3\ \mathrm{GeV}^2) = 0.0057 \pm 0.0009 \pm 0.0007$ is significantly above zero. In the Update section we'll compare these results with the expected SANE measurement. There are no other lattice QCD calculations for the proton d_2 except the one cited.

In addition to lattice QCD, QCD sum rules [28, 29, 30], bag [31] and chiral quark models [32, 33] can also be tested by comparing their predictions to the measured moments of g_2. Moreover, g_2 gives access to the polarizabilities of the color fields [34] (with additional knowledge of the twist-4 matrix element f_2). The magnetic and electric polarizabilities are $\chi_B = (4d_2+f_2)/3$ and $\chi_E = (2d_2-f_2)/2$, respectively. Knowledge of these properties of the color fields is an important step in understanding QCD. The twist-4 f_2 matrix element represents quark-quark interactions, and reflects the higher twist corrections to the individual proton and neutron moments of g_1 and in consequence, to the Bjorken sum rule [35]

$$\int_0^1 g_1(x,Q^2)dx = \frac{1}{2}a_0 + \frac{M^2}{9Q^2}(a_2 + 4d_2 + 4f_2) + O\Big(\frac{M^4}{Q^4}\Big). \tag{3}$$

These matrix elements are related to the higher moments of the SSF's, which have a strong dependence on the high x contributions.

From an experimental point of view, the measurement of A_2 is simpler than that of the absolute cross section difference for scattering of longitudinally polarized electrons on transversely polarized nucleons, which is required to access g_2 directly. Therefore, it is easier to measure the parallel $A_\parallel$ and perpendicular $A_\perp$ asymmetries which are related to the spin asymmetries A_1 and A_2 by

$$\begin{aligned} A_1 = &\quad \frac{1}{(E+E')D'}\Big((E - E'\cos\theta)A_\parallel - \frac{E'\sin\theta}{\cos\phi}A_\perp\Big) \\ A_2 = &\quad \frac{\sqrt{Q^2}}{2ED'}\Big(A_\parallel + \frac{E - E'\cos\theta}{E'\sin\theta\cos\phi}A_\perp\Big) \end{aligned} \tag{4}$$

where all quantities (θ and ϕ are the scattered lepton's polar and azimuthal angles, respectively) are measured in the same experiment, with the exception of the small contribution from the unpolarized structure function $R(Q^2,W) = \sigma_L/\sigma_T$ to the virtual photon depolarization $D' = (1-\varepsilon)/(1+\varepsilon R)$. Here $\varepsilon = 1/(1 + 2(1+\nu^2/Q^2)\tan^2(\theta/2))$ is the well known longitudinal polarization of the virtual photon. These expressions are suitably modified for the case when the beam and target spins aren't exactly perpendicular.

As discussed in the original (year 2003) version of this proposal [36], at that time there was a stark dearth of data on $A_\parallel$ and, particularly, $A_\perp$ in the region of the (Q^2,x) kinematic plane for $x >\sim 0.6$. This region is entirely dominated by the nucleon resonances for $Q^2 \leq 5$ GeV^2. Since

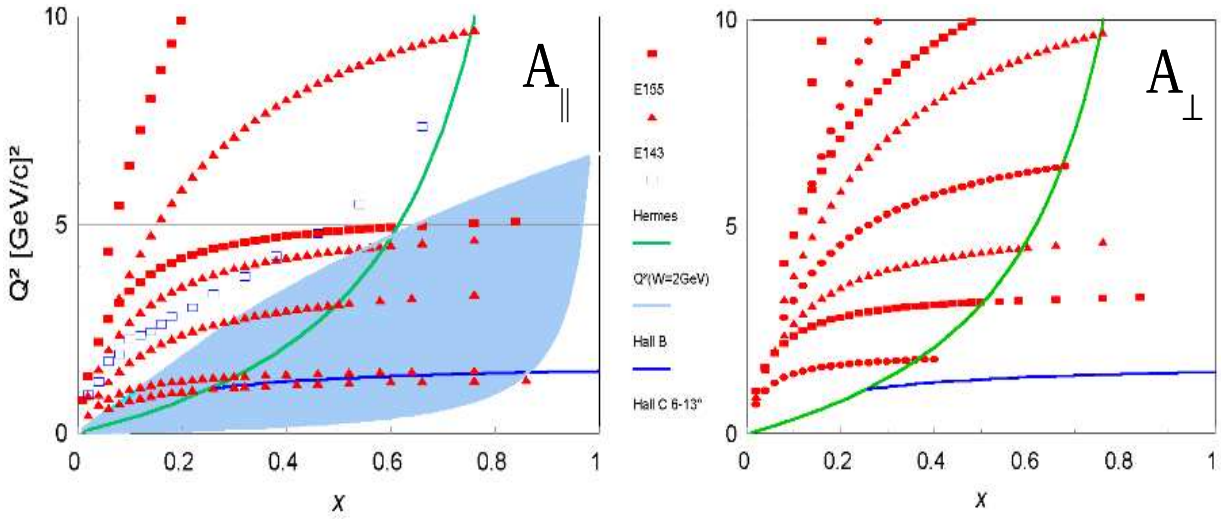

Figure 1: Central kinematics of DIS $A_\parallel$ (left) and $A_\perp$ (right) measurements on protons and deuterons, for $0 \leq Q^2 \leq 10$ GeV^2. The region of $W > 2$ GeV lies to the left of the solid (green) curve. The shaded region (Hall B) and the thick (blue) line (Hall C RSS) represent the only new measurements since this experiment was approved in 2003.

then, only parallel asymmetry results for protons [18, 16, 20] and deuterons [18, 16, 20] have become available for most of the region. The only perpendicular asymmetry measurement on protons and deuterons was done by the *RSS* collaboration in Jefferson Lab's Hall C [20, 37] and it is limited to the resonances at $< Q^2 > \sim 1.3$ GeV^2. The situation for these two targets is illustrated in Figure 1, where the absence of $A_\perp$ data at high x is glaring. It should be said that the situation is somewhat better for the neutron, for which a dedicated g_2 DIS measurement [38] and a spin duality study [21] have been done in Hall A.

The importance of $A_\perp$ data in obtaining reliable results for all the SSF's, not just g_T, cannot be underestimated. Although in DIS kinematics the approximate relation $A_1 \approx g_1/F_1$ is frequently applied, it is only valid when the coefficient of g_2 is much smaller than unity in the exact expression

$$A_1 = \frac{1}{F_1}\Big(g_1 - \frac{(2Mx)^2}{Q^2} g_2\Big), \tag{5}$$

It is straightforward to see that at $Q^2 \leq 6$ GeV^2 this coefficient is greater than 0.2 for $x > 0.35$, with the obvious implication that a significant systematic error may be introduced if the g_2 contribution is neglected because it is assumed to be small. The equivalent error may be made when attempting to obtain A_1 from only parallel asymmetry data. Figure 2 illustrates the difference between true $A_1(A_\parallel, A_\perp)$ obtained in *RSS* [20] and the approximation $A_1 \sim A_\parallel/D$: the contribution of A_2 is not negligible, even when suppressed by the coefficient $\eta \sim 0.5$ at *RSS* kinematics.

While the experimental situation for $A_\perp$ remains unchanged, the importance of gaining complete knowledge of the nucleon spin structure grows with time. The need for precise spin structure function data, g_T in particular, may be best illustrated by the fact that one of DOE's 2011 milestones of the Performance Measures for Hadronic Physics [39] is to measure the proton spin structure functions g_1 and g_2 over the kinematic range delimited by $0.2 < x < 0.6$ and $1 < Q^2 < 5$ GeV^2.

The above considerations, and others which are discussed in detail in the original SANE proposal, make it clear that precise measurements of the SSFs in the region of $x > 0.5$ are required for

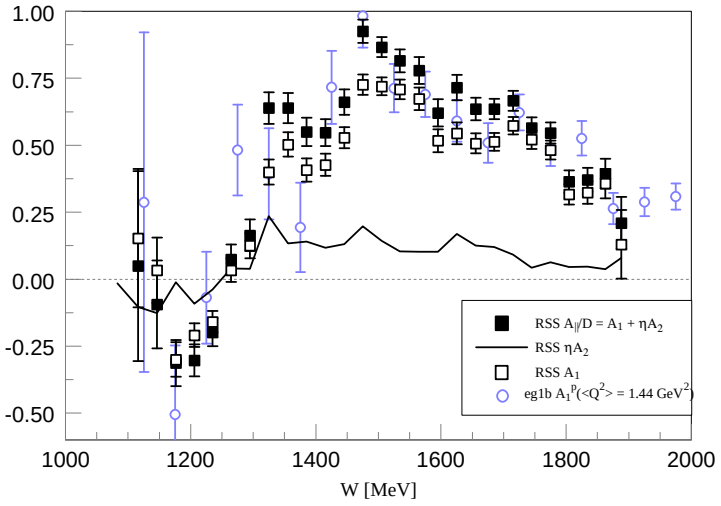

Figure 2: Proton A_1 approximated by $A_\parallel/D'$ (solid squares) measured in *RSS* [20] ($Q^2 \simeq 1.3$ GeV^2) and exact A_1 (open squares). The contribution of A_2, suppressed by η (~ 0.5) is shown as the solid curve. Hall B results [16] from $A_\parallel$ at nearby kinematics ($Q^2 \simeq 1.4$ GeV^2) are also shown (open circles). All errors are statistical only.

further progress in our understanding of the nucleon and the interactions among its components.

On the theoretical side, progress in our understanding of g_2 has also been slow in the past few years, likely due to the absence of data. The recent extensive review by Bass [40] on the proton spin structure devotes only a less than one page long section to g_2, discussing mainly older results. It is evident that further progress will necessitate experimental input.

2 Statement of intent to renew E-03-109

With this update document we reiterate our proposal (conditionally approved as TJNAF E-03-109 - SANE) to carry out a measurement of the proton spin structure using the Jefferson Lab CEBAF and Hall C facilities and the UVa polarized target. The goal of the proposal is to extract the proton A_1 limited by systematic errors and a simultaneous statistics limited measurement of g_2^p in the range $0.3 \leq x \leq 0.8$ at an average Q^2=4.5 (GeV/c)^2 in a model-independent fashion, from the measurement of two asymmetries for two different orientations of the target magnetic field relative to the beam direction. SANE will meet or exceed DOE's 2011 milestone of the Performance Measures for Hadronic Physics, by measuring the proton spin structure functions g_1 and g_2 over a wider kinematic range than that indicated for the milestone.

JLab is the only facility in the world where these measurements can be carried out, because of the concurrence of three critical factors:

– the high polarization CEBAF beam;

– the very large solid angle of the proposed Hall C Čerenkov plus calorimeter plus tracking hodoscopes detector system, BETA ("**B**ig **E**lectron **T**elescope **A**rray"), which makes possible high

statistics measurements at $Q^2 \sim$ 5 GeV^2 in reasonable amounts of run time;

– the open geometry of the UVa solid polarized target, that allows for flexible relative orientations of the beam helicity and the target spins, coupled with the high proton polarizations($\geq$ 75% average) that it can attain.

The measured A_1 and g_2 will be used directly to:

- study their x dependence at constant Q^2, and Q^2 dependence at fixed x, in both the DIS and resonance region
- determine $\overline{g}_2$ with high precision in the critical region $0.3 \leq x \leq 0.8$ at fixed Q^2, and compute d_2 combining SANE and world data
- extract better values of g_1 from A_1 and A_2 with the aid of the unpolarized structure functions F_2 and R to further improve the calculation of moments
- probe the approach of A_1 to $x = 1$ at constant Q^2 in order to test quark models and pQCD, combining SANE's results with the world data sample,
- conduct a limited test of local duality for the polarized SSF's down to the second resonance region.

In what follows we give a progress report on the work on the experiment subsystems and plans for absolute calibrations that our collaboration has carried out since PAC24, and conclude with summaries of our collaboration status and beam request.

The choice of kinematics and technique, the basic detector design and their response to electrons and background, the polarized target and auxiliary equipment, are described in the original SANE proposal, where we also give estimates of the expected count rates, statistical precision and systematic errors. We refer the readers of this update to that proposal, which is included as part of this submission. We conclude with summaries of the collaboration status and of our beam request, including a preliminary run plan and installation requirements.

3 Update

Although the experimental and theoretical situation regarding g_T has experienced little change since the conditional approval of E-03-109 by PAC25, there have been changes in the capabilities of the CEBAF machine that have some impact on the proposed measurements. Also, the reference design of the BETA detector has evolved significantly, with the goal of improving its resolution and background rejection characteristics. The SANE collaboration has grown substantially and collaborating groups have been busy, either building the BETA detector subsystems or prototyping them, and planning the required calibration and data taking procedures. This work is driven by a commitment to be ready for installation and data taking in the first half of 2008. The management of Hall C has been very supportive, with funds, access to facilities, parasitic test runs and inclusion of SANE in the Hall's long term schedule. Before proceeding to give a detailed description of the more important items on BETA and the experiment, it is helpful to give a brief review of the experiment.

SANE will measure inclusive double spin asymmetries by scattering polarized electrons on polarized protons, in the range of Bjorken x from 0.3 to 0.8 and the corresponding range of four-momentum transfer from 2.5 to 6.5 GeV^2. Beams of about 6 GeV and 4.8 GeV will scatter off solid ammonia material placed in the UVA-Basel-JLab polarized target. The target polarizing field will be aligned parallel to the beam at 80° to the left of the beam, to measure $A_\parallel$ and near-$A_\perp$.

Obstruction of the scattered electrons by the target magnet coils necessitates the 80° alignment, which has only a minor effect in the optimal extraction of A_1 and A_2 from the conventional exactly orthogonal asymmetry.

The scattered electrons will be detected in the novel non-magnetic very large solid angle BETA detector centered at 40°, covering ±10° of horizontal acceptance. BETA's primary subsystem is the BigCal lead glass electromagnetic calorimeter that has been constructed for the measurement in Hall C of the ratio of the proton's electric to magnetic form factors at large Q^2, $GEp-III$ [41]. A threshold gas Cherenkov and two tracking hodoscopes will augment the particle identification, vertex resolution and background rejection of BigCal. The expected performance of BETA is 1000:1 pion rejection ratio, vertex resolution of 0.5 cm (worst case resolution < 5 cm with only the Lucite hodoscope operational), angular resolution of ~ 1 mr (worst case 0.8°), and very good rejection of Hall background. BigCal will be outfitted with a continuous gain monitoring system, which is being built by our collaboration and will already be in place for the $GEp-III$ run.

The overall configuration of BETA has basically not changed from the reference design described in the original proposal [36], except for the addition of a forward high resolution tracking hodoscope, situated between the polarized target's outer vacuum can (OVC) and the upstream window of the gas Cherenkov.

The collaboration has been working to build a detector that addresses the concerns about backgrounds at the root, namely by having a robust system with redundancy and adequate resolution to reject events not originating at the target. Beyond that, the front tracking hodoscope will have the ability to determine the sign of the low momentum electrons, which contribute most of the pair symmetric background. Testing of prototypes and full detectors in beam conditions comparable to those expected during SANE are planned for 2007 for the gas Cherenkov and the two hodoscopes, complementing the work done in 2005 for the gas Cherenkov. This work should go a substantial way to meet the conditions stated in the PAC24 report on SANE.

On the software side, work on a fully detailed GEANT simulations of the experiment and of the expected possible beam line background are ongoing. The collaboration plans to combine the strengths of the packages developed for SANE and $GEp-III$ into a comprehensive tool.

What has changed:

- The maximum beam energy that the CEBAF will be able to deliver by early 2007 is expected to be $E <\sim 5.8$ GeV, not the proposal's 6 GeV. As a result, there will be a small reduction of kinematic range for the maximum value of Bjorken x for which the final state mass $W > 2$ GeV. On the other hand, the event rates at the resulting slightly smaller Q^2 will lead to a commensurate improvement in collected statistics. The difference between the kinematics for each beam energy is illustrated on figures 3 and 4. As expected, there is only a small shift of the distributions toward smaller Q^2 at a given x.

  We have explored the effects of the lower energies in the expected uncertainties for the measured $\overline{d}_2(Q^2)$, as the most representative indicator. Table 1 shows the values of the average Q^2 for the data intervals from 2.5 to 6.5 GeV^2 in steps of 1 GeV^2, ranges of x and expected statistical error in $\overline{d}_2$ for both kinematic settings. For comparison, the results from the SLAC and RSS measurements and the lattice QCD calculation are also shown. The last two rows show the numbers for the combination of SANE data from 3.5 to 6.5 GeV, which have a broader x range than the three individual Q^2 intervals, minimizing the unmeasured range. As the table shows, the reduction in the beam energies has only a small impact, mainly reflected in the shrinking of the x range at the higher Q^2. It should be mentioned that the binning in $\Delta Q^2 = 1$ GeV^2 bins is illustrative only; the actual binning will be done by optimizing the widths to yield the smallest overall errors, including contributions from unmeasured regions

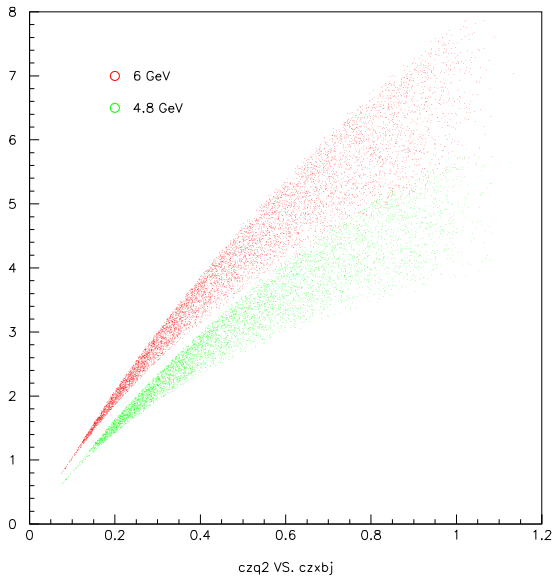

Figure 3: Distribution of GEANT reconstructed events in the Q^2 vs x plane for BETA at 40° and beam energies of 6 GeV (top band) and 4.8 GeV (bottom band). A cut on the inclusive $e-p$ cross section > 0 has been applied.

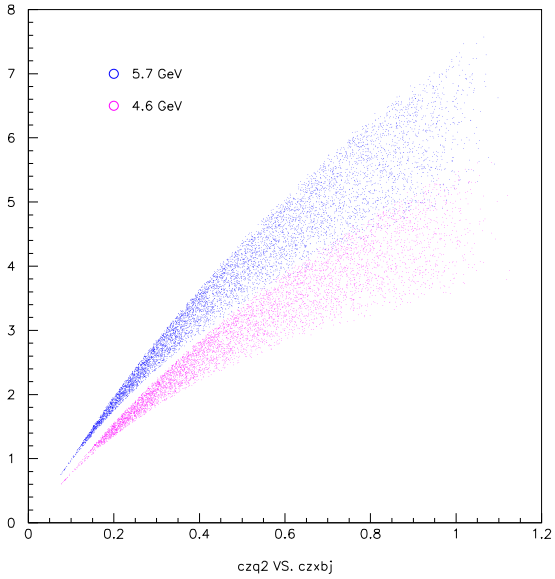

Figure 4: Same as graph on left, but for beam energies 5.7 GeV (top band) and 4.6 GeV (bottom band).

and systematic errors.

The tabulated numbers come from the output of the GEANT simulation of the response of the BETA detector, with a software cut on scattered electron energy $E' \geq 1.3$ GeV, to keep the contamination from pair symmetric background small. The addition of the forward tracking hodoscope which is expected to identify the sign of the electron charge should make this restriction unnecessary, leading to an increase in the statistics at low x. The rates used in the simulation are based on the MRST parameterization of parton distribution functions [42], and are the only model-dependent input, aside from the usual geometric and material properties inputs used in GEANT. The uncertainties are based on the PAC24 approved running times for each configuration: 200 h at 6(5.7) GeV and 100 h at 4.8(4.6) GeV for 80° data, and 130 h at 6(5.7) GeV and 70 h at 4.8(4.6) GeV for the parallel data.

Figure 5 gives a graphical illustration of the expected errors on $\overline{d}_2$, plotted on top of a simple phenomenological form for $d_2(Q^2) = \overline{d}_2(RSS)\sqrt{Q^2(RSS)/Q^2}$, which is anchored at the RSS result. The elastic contribution to d_2, the SLAC measurement and the lattice QCD result are also plotted.

The expected systematic uncertainties for SANE haven't changed from the conservative ones given in the original proposal's table 7. Experience with actual measurements of d_2 in Hall C indicates that these expectations are well founded, as demonstrated in RSS.

The collaboration has taken the beam energy limitation into account in the planning of the calibrations, beam transport, radiation budget, target's OVC design, etc. Only linac energies in integer multiples of the one that delivers $\sim$ 5.7 GeV in 5 passes have been used in the calculations.

Experiment	**<Q²>** GeV²	***x* low**	***x* high**	**stat. d2bar error**	**d2**	**total d2 error**
SANE 6 GeV	3.12	0.28	0.74	0.00069		
	4.07	0.39	0.95	0.00044		
	4.89	0.50	0.96	0.00039		
	5.91	0.64	0.93	0.00029		
SANE 5.7 GeV	3.12	0.29	0.85	0.00073		
	4.06	0.41	0.96	0.00039		
	4.99	0.53	0.96	0.00040		
	5.89	0.69	0.92	0.00028		
SLAC E155x	5	0.02	0.8	0.0016	0.0025	
SLAC E155	5	0.02	0.8	0.0080	0.0050	
SLAC E143	5	0.03	0.8	0.0050	0.0058	
SLAC (all)	5	0.02	0.8		0.0032	0.0017
RSS	1.3	0.29	0.84	0.0009	0.0057	0.0012
Lattice QCD	5				0.0040	0.0050
SANE 6 GeV	5.23	0.39	0.96	0.00020	(Avg. of top 3 Q² pts.)	
SANE 5.7 GeV	5.19	0.41	0.96	0.00020	"	

Table 1: Expected statistical uncertainties in the measured $\overline{d}_2$ for four intervals of Q^2 from 2.5 to 6.5 GeV^2 in 1 GeV^2 steps for beam energies of 6 GeV and 5.7 GeV. SLAC, *RSS* and lattice QCD results are also shown. The last two rows combine SANE data for Q^2 from 3.5 to 6.5 GeV^2.

- As briefly mentioned above, we have added a front, or forward, hodoscope to improve tracking, background rejection, and distinguish electrons by charge for some kinematics.
- We have redesigned the reference design's Lucite hodoscope, which we are preserving as part of BETA for redundancy with the new, more precise, front hodoscope.
- The gas Cherenkov is based on Temple U.'s design, which optimizes the collection and focusing of light on a single row of 3" photomultipliers located on the side far from the beam line. This detector is being built with Temple University funds.

Brief reports on each subsystem are give next.

4 Status of BigCal

The large calorimeter, BigCal, has been assembled in the Test Lab at Jefferson Lab. BigCal is presently being tested using a cosmic ray trigger. Before SANE runs, BigCal will be used in experiments E04-108 ($GEp-III$) and E04-019. SANE collaborators will take part in E04-108 and

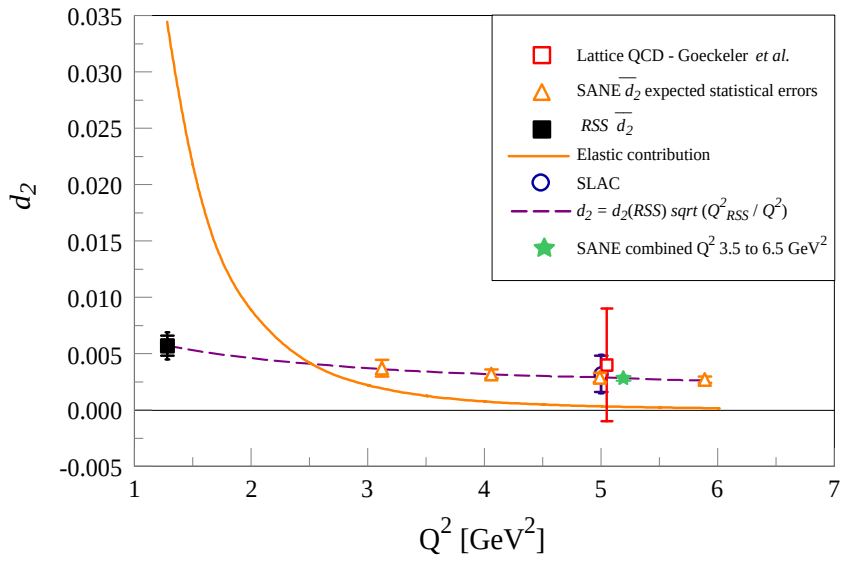

Figure 5: Expected SANE $\overline{d}_2$ results for 5.7 GeV beam energy (open triangles) plotted on top of $d_2(Q^2) = \overline{d}_2(RSS)\sqrt{Q^2(RSS)/Q^2}$ (dashed curve). The solid star represents the combination of the three highest Q^2 SANE points. The *RSS* (solid square) with statistical and combined error bars, SLAC (open circle) with total error, and lattice QCD (open square) results are also shown. The solid curve is the elastic contribution to d_2.

E04-019 to gain experience in operation of BigCal. A short description of BigCal is given in section 3.1.3 of the SANE original proposal.

The trigger for BigCal has been designed. The electronic components have been purchased. The trigger is assembled and is being used as the cosmic trigger in the Test Lab. The trigger will be used during E04-108 and E04-019 in coincidence with the HMS trigger. A description of the trigger follows.

The calorimeter consist of 56 rows and 32 columns. Each photo-tube signal is input to a first level summing module (designed and manufactured at Rutgers University) which accepts 8 inputs. Each first level trigger sums 8 photo-tubes and each row divides into 4 first level summing modules. In Fig. 6, these sections of rows are labels A,B,C and D. There are 224 first level summing modules. In the module, the 8 individual inputs are amplified by 5 and output individually in the back of the unit. These amplified individual signals go to an ADC. In addition, the module sums the eight inputs and produces 6 summed output signals. One output signal will go to a discriminator and then a TDC. Another output channel will go to the input of the second level summing module and be summed with the output of 7 other first level summing modules. The second level summing module does not amplify the individual input signals and produces six summed output signals. The output of the second level summing module is the sum of 64 photo-tubes. An example of the trigger logic is shown in Fig. 7, where the second level summing module sums the signal from sections A and B (columns 1-16) for rows 1 through 4. To have overlap, the next second level summing module

sums the signal from sections A and B (columns 1-16) for rows 4 through 7. This continues for the right half of BigCal and the same is done for the left half. There is no overlap between the halves of BigCal, which leads to a slight loss in trigger efficiency. A total of 39 second-level summing modules are needed to cover BigCal. Each individual output signal is sent to a discriminator and the "OR" of the 39 signals is the trigger.

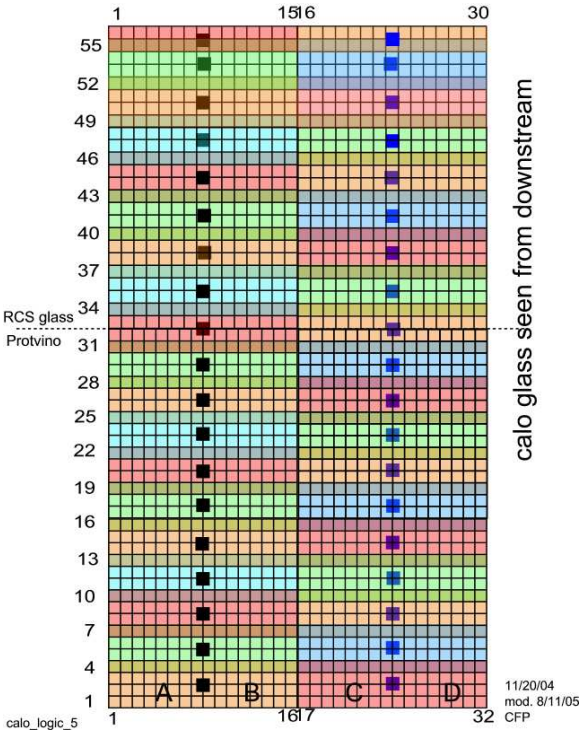

Figure 6: A rear view of the lead-glass in the BigCal calorimeter.

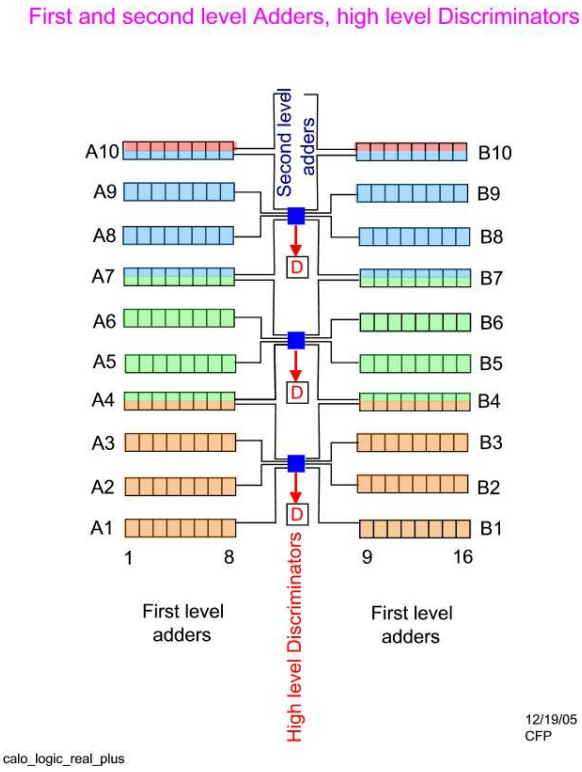

Figure 7: A diagram of the trigger logic

To examine, the effect of non-overlap between the left and right halves of BigCal, a GEANT Montecarlo was run which simulated the response of BigCal and the trigger setup. In the Montecarlo, 1.2 GeV electrons were incident on BigCal with a 10 cm aluminum plate in front. The plate is needed during E04-108 and E04-019, but won't be used for SANE. Fig. 8 shows the trigger efficiency as a function of discriminator threshold. For a threshold of 700 MeV, trigger efficiency is about 95%.

The main experiment trigger will be formed as the AND function between the BigCal OR and the Cherenkov OR.

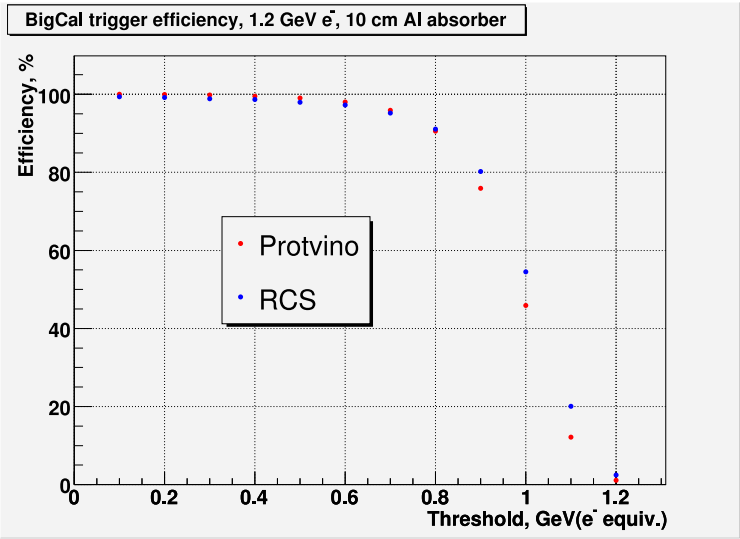

Figure 8: Trigger efficiency versus discriminator threshold. The "Protvino" is the lower section of BigCal and " RCS" is the upper section.

5 BigCal Gain Monitoring System

Design of the proposed BigCal gain monitoring system draws on experiences acquired with the JLab Radphi lead glass detector (experiment E94-026) and analyzing the collected monitoring and calibration data [43]. The monitoring setup based on using a single Plexiglas plate as a light distributor originated with the BNL experiment E852 [44]. The independent Monte Carlo simulations confirmed the uniformity of the light response even for a simple prototype system [45].

The BigCal gain monitoring system will be used to: (i) obtain the relative gain-versus-high-voltage characteristics for each calorimeter phototube, (ii) confirm proper PMT/voltage divider operation as the calorimeter is powered up, and (iii) initiate a warning if any PMT signal stops reporting during data collection. We will further expand the system to monitor fast trigger components, in addition to monitoring temporal gain variations of individual calorimeter modules, and providing the initial gain constants for the energy calibration software.

The gain monitoring sub-system of the BigCal calorimeter will consist of: (i) a stable light source (LED - light-emitting diode or laser), (ii) a set of optical fibers acting like light guides, (iii) a clear Plexiglas plate cut to fit the front face of the calorimeter, and (iv) a photodiode used for absolute light normalization. A simplified layout is shown in Fig. 9. The system is self-contained and could be serviced without interfering with the calorimeter operation. While expected pulse-to-pulse LED/laser light output variation is $\leq 1\,\%$, a stable photodiode will be used to provide the absolute normalization. The $\sim 1\,\mathrm{Hz}$ monitoring trigger will be interlaced with the physics triggers.

The 1 inch thick clear Acrylic plate of radiation resistant Acrylite FF type for the final system will be ordered shortly from the Cyro Industries [46]. The light will be provided via 2×56 optical fibers coupled to the opposite long sides of the plate. We expect that arrangement to result in less than $30\,\%$ variation in light intensity across the $140\times239\,\mathrm{cm}^2$ surface of the plate. We will cross-calibrate the light response of the plate in-situ using cosmic muons and a Monte Carlo simulation. We will also consider calibrating the plate independently, by moving an individual lead

glass detector module across its surface. We plan to check for possible temperature variations in light output using both LED and laser-based drivers. Design of the light-tight enclosure has also been initiated, Fig. 10.

For the light source we have a choice of using the custom-build LED system currently operational in the JLab test lab or the Nitrogen laser system, last time used in 2001 in G_E^n experiment in the Hall C [47]. A Photonics Corp. LN-127 337 nm N2 laser was installed in the Hall C counting house in a special shielding box. The light intensity could be regulated by means of filters. The laser light with the original wavelength or wave-shifted to ~ 400 nm would be transported down into the Hall C by 1 mm diameter silica fiber. Next to the spectrometer axis the two stages of light-splitters divide the source light into up to 160 secondary optical fibers. Most of the assembly parts from the earlier experiment should still be available. The new operating safety procedure for the updated system would have to be written.

We are also relying on using the University of Virginia Photonics LN120C laser as a backup unit. The UVa laser, complete with its shielding box, a gas regulator and optical fiber light distribution system, has already been transported to JLab.

In the JLab test lab we have examined the signal amplitudes and gain stability of the PMTs coupled to the individual lead glass modules using a smaller prototype system covering one quarter of the BigCal front face. The system had $1.27\times99\times175\,\mathrm{cm}^3$ Plexiglas G plate and a custom-built LED light distribution system with 25 light-feeding fibers, Fig. 11. We have ascertained that the amount of light delivered to the PMTs is well above the pedestals and noise levels and is sufficient for the monitoring and calibration purposes.

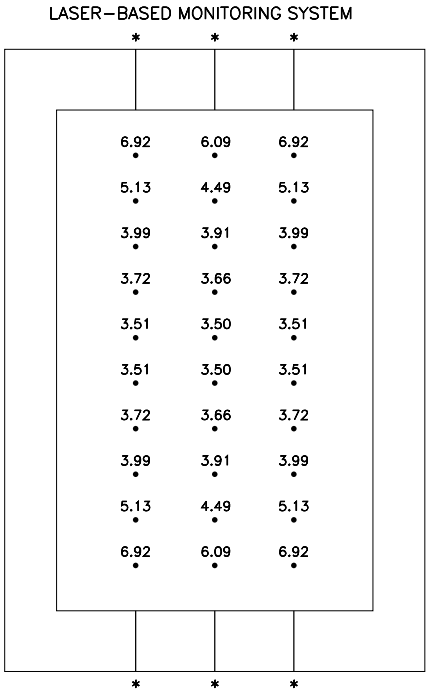

Figure 9: The simplified layout of a gain-monitor system based on a prototype $1.27\times99\times175\,\mathrm{cm}^3$ Plexiglas plate. The six thin (1 mm ϕ) optical fibers (top and bottom) feed the light from the source into the plate volume. The numbers shown represent the measured light output as a function of the PMT position [43].

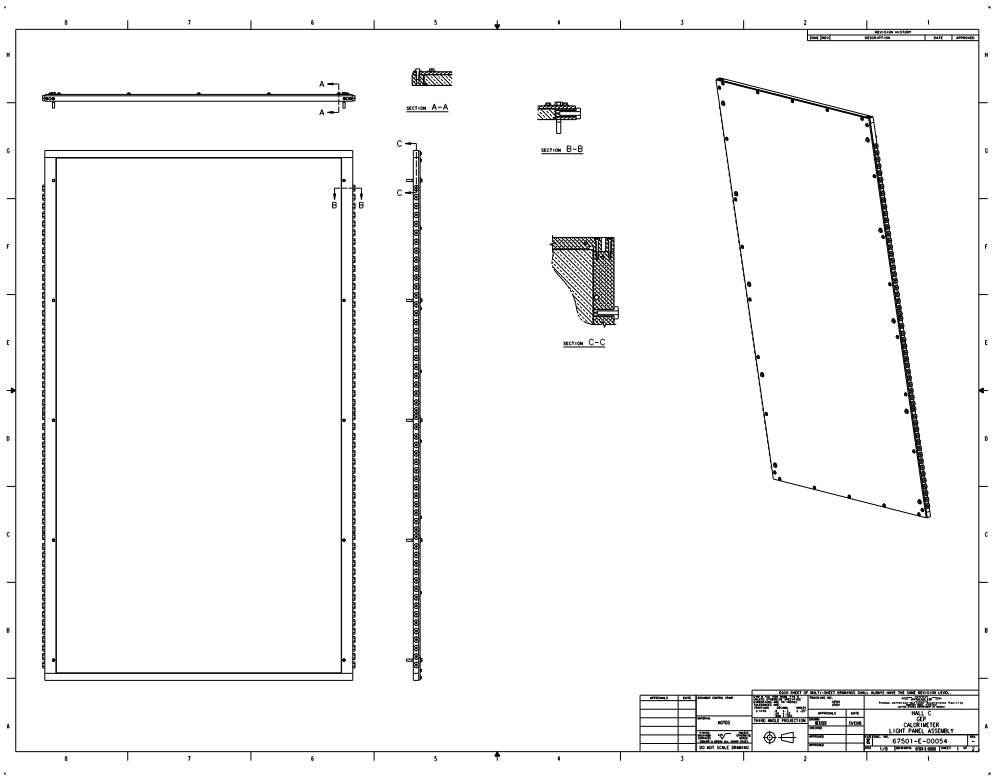

Figure 10: Proposed design of the light-tight enclosure housing the gain monitoring plate.

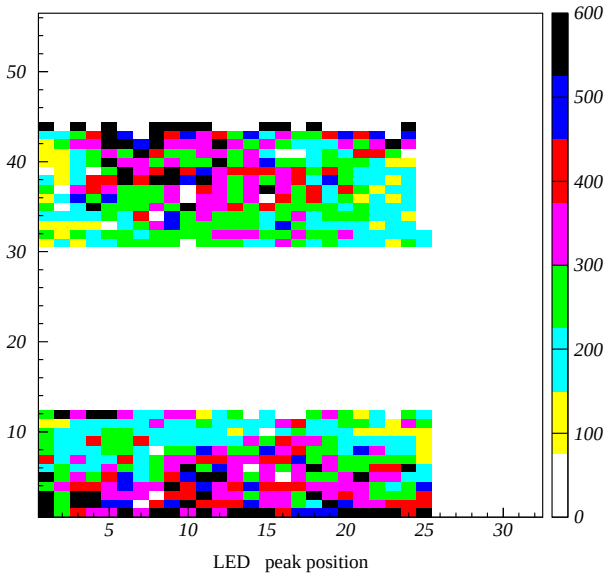

Figure 11: Signal peak positions measured in the individual BigCal channels. The smaller prototype Plexiglas plate, covering a fraction of the lead glass detectors, was excited with a custom-built LED system. The size of the plate in calorimeter channels is 1→25 horizontally and 1→43 vertically. Not all channels were supplied high voltages, hence the missing channels.

6 Elastic Calibrations

As the asymmetry measurement uses only a single-arm, it is highly desirable to obtain an absolute energy calibration of the BETA spectrometer via the $e + p$ elastic scattering reaction. Protons detected in the HMS in coincidence with BETA will be used to define electrons of known energy in the calorimeter. The constraints in selecting the appropriate kinematics for these calibrations are: the deflection of the incident electron beam in the target magnetic field, the limitation in the proton and electron angles caused by the magnetic field coil obstruction, and the desirability of a calibration with electrons of 0.8-2.2 GeV energy similar to those used in the asymmetry measurement. Of the various beam energies available with a 5 pass=5.7 GeV linac tune, only the 2 pass=2.32 GeV setting is compatible with these constraints. Therefore, a special beam energy is required for these calibrations. As the target material will not be polarized, it will be possible to increase the beam current to 1 μA to increase the calibration counting rate and reduce the total beam time required.

These energy calibrations will be obtained with the target field aligned parallel and anti-parallel to the electron beam. Thus, even though the beam energy is relatively low, the beam will be undeflected. In this target orientation, scattering angles from $\pm 50^o$ are unobstructed, and a number of HMS angle settings can be used to define 1-2 GeV coincident electrons across the full horizontal range of the calorimeter. The planned kinematics are listed in Table 2. HMS angle scans with parallel and anti-parallel fields will allow calorimeter blocks 35 cm below and above beam height to be calibrated. A third scan with the field off will calibrate those in the middle, as well as to allow the dependence of the calibration upon magnetic field orientation to be studied. These are shown in Fig. 12, about 75% of the calorimeter can be calibrated in this manner. Two additional scans with parallel and anti-parallel fields at half strength (2.55 T) can fill in the gaps in-between, raising the fraction of the calorimeter to be calibrated in this manner to approximately 90%.

The anticipated elastic coincidence rates per 4×4 cm^2 crystal are listed in Table 2. As expected, the coincidence rate drops quickly as Q^2 is increased. Taking 400 elastic counts per 4×4 cm^2 crystal as the desired minimum for the calibration, we estimate that the entire study will take 3.3 days of beam (at 60% data-taking efficiency), of which 2 days are for the full field plus field off part, and the remainder for the half-field setting. Additional time will be required for the target and linac setup, which is part of the commissioning and calibration schedule.

We have also investigated the use of the 4.6 and 5.7 GeV electron beams to parasitically monitor the energy calibration during the asymmetry measurements. At these energies, the $e + p$ elastic cross section drops even more steeply with angle, so the low rates preclude the use of more than a single HMS angle per beam energy. Some kinematics which are under consideration for the parasitic calibration monitor are listed in Table 3. We anticipate only a few dozen coincidences per crystal per 100 hours of asymmetry running. Perhaps the most important use of these events will be to provide two higher energy calibration points to verify the linearity of the calorimeter energy calibration. By summing over several dozen adjacent crystals (a small fraction of the 1744 available), the necessary statistical precision for this check could be obtained. In addition to providing an absolute energy calibration, these coincidence data could be used to measure the target packing fraction by comparing to the known $e+p$ elastic cross sections. In this case, one might sum over adjacent crystals to improve the statistical precision of the packing fraction measurement.

In addition to the elastic calibrations, the entire calorimeter will be cross-calibrated by π^0 mass reconstruction during the asymmetry measurements, as was discussed in the original proposal's section on "Gain Monitoring".

The HMS will also be used for part of the time to measure the rate of positron events as a function of scattered energy, to complement the charge sign identification provided by the forward tracking hodoscope.

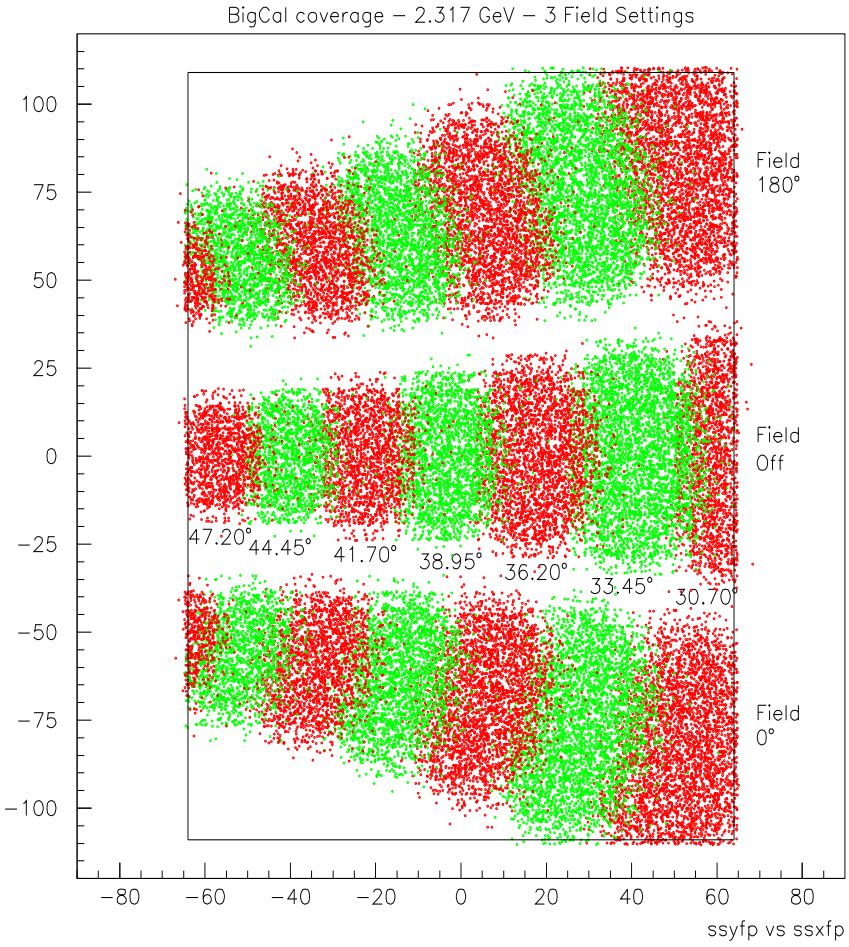

Figure 12: Simulated locations of electron hits across the calorimeter for the various HMS (proton) angle settings and target field orientations listed in Table 2. The half-field settings are not shown. BETA is set at an angle of 40^o and 320 cm from the target throughout.

2.32 GeV $e+p$ elastics										
$E_{e'}$	$\theta_{e'}$	Q^2	θ_p	p_p	Counts/cell/hr			Beam time (hrs)		
(GeV)	(deg)	(GeV^2)	(deg)	(GeV)	0^o Field	180^o Field	Field Off	0^o Field	180^o Field	Field Off
1.92	30	1.07	47.20	1.19	1810	1820	6800	0.3	0.3	0.1
1.66	33	1.22	44.45	1.29	1860	1820	1980	0.3	0.3	0.3
1.58	36	1.38	41.70	1.39	1010	1010	1090	0.4	0.4	0.4
1.49	39	1.55	38.95	1.50	560	550	600	0.8	0.8	0.7
1.39	43	1.73	36.20	1.61	310	300	330	1.3	1.4	1.3
1.29	47	1.92	33.45	1.72	160	170	180	2.5	2.4	2.3
1.19	50	2.11	30.70	1.84	94	95	104	4.3	4.3	3.9
Half-Field Rates										
1.92	30	1.07	47.20	1.19	3140	3160		0.2	0.2	
1.66	33	1.22	44.45	1.29	1950	1910		0.2	0.2	
1.58	36	1.38	41.70	1.39	1080	1070		0.4	0.4	
1.49	39	1.55	38.95	1.50	590	580		0.7	0.7	
1.39	43	1.73	36.20	1.61	325	320		1.3	1.3	
1.29	47	1.92	33.45	1.72	175	180		2.3	2.3	
1.19	50	2.11	30.70	1.84	103	102		3.9	3.9	
Total Time (100% efficiency)								19	19	9

Table 2: Elastic scattering kinematics and projected BETA+HMS coincidence rates as determined from a SIMC simulation including the effect of the 5.1 T target magnetic field, the beam slow raster, etc. The proton is detected in the HMS and the scattered electron is in BETA, which is positioned at 40^o and 320 cm from the target throughout. The rates are per hour per 4×4 cm^2 cell assuming a beam current of 1 μA and the 3 cm target.

Parasitic energy monitor settings									
E_{beam}	$E_{e'}$	$\theta_{e'}$	Q^2	θ_p	p_p	counts/cell/100 hr		Total counts/100 hr	
(GeV)	(GeV)	(deg)	(GeV^2)	(deg)	(GeV)	80^o Field	180^o Field	80^o Field	180^o Field
4.57	1.98	43	4.86	23.40	3.40	36	37	5830	5340
5.70	2.53	37	5.95	22.60	4.00	18	20	2530	2380

Table 3: Elastic scattering kinematics which could be used as a parasitic calibration monitor during the physics data-taking. The rates are per 100 hours per 4×4 cm^2 cell assuming a beam current of 85 nA and the 3 cm target.

7 Threshold Čerenkov counter for SANE

Design Considerations

The principal requirements for the Čerenkov counter are to provide high efficiency (greater than 90%) for electron detection while maintaining a pion rejection factor of at least 1,000:1. A gas Čerenkov is the logical choice because the low areal density minimizes the probability of δ-rays from π and e scattering.

Firstly, operation at atmospheric pressure is assumed in order to simplify the mechanical design and minimize the windows thicknesses. The choice of radiator gas is a trade-off between many parameters. The reference design assumes the use of dry N_2 gas. At 20° C, the index of refraction

n of N_2 is approximately 1.000279, yielding a β threshold for Čerenkov light emission by pions of

$$\beta_{threshold} = \frac{1}{n} = 0.999721,$$

which corresponds to a momentum threshold for pions of 5.9 GeV/c. Pions above this momentum threshold should be extremely rare with 6 GeV beam and would be removed in any case with our software electron definition, >3-5 photoelectrons. This cut will also suppress low energy δ rays and virtually extinguish expected scintillation backgrounds from all non-electron charged particle species. Desiccants will be placed in the radiator box, it will be flushed with dry N_2 to remove contaminants, and then hermetically sealed with a slight overpressure (1 cm of water equivalent). A thin front window of Tedlar will provide a light-tight seal. An interior polymer window will provide a gas-tight seal capable of withstanding normally variations in barometric pressure (± 1" of water equivalent).

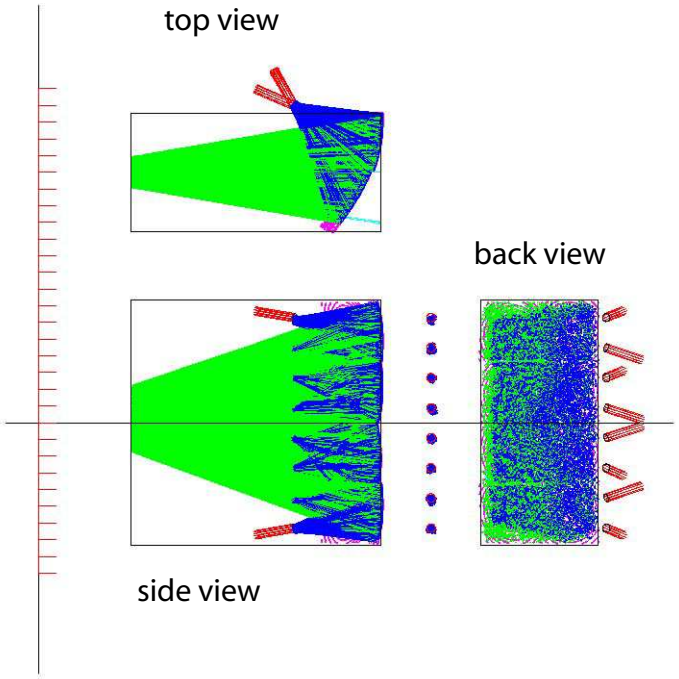

Figure 13: Optical ray trace analysis of Cherenkov light reflected from the mirrors to the PMT's

After an extensive detailed optical ray-trace analysis (see Fig. 13) which included among other things the effect of the target magnetic field on the scattered electron trajectories, the shape of the mirrors were determined. The optimized result called for eight, roughly 40 cm by 40 cm glass mirrors arranged in two overlapping columns of four mirrors to cover the rather large acceptance shown in Fig 14. Four spherical mirrors will cover one column at large scattering angle and four elliptical mirrors will cover another column at small scattering angle. Light from each mirror will be focused onto individual 3" quartz window photomultipliers (Photonis XP4318B) without the use of a Winston cone. The 3" size helps reduce background signals generated on the photomultiplier. It also provides for more space to shield from the magnetic field of the target magnet with thicker μ-metal jackets. All phototubes will be located on the large scattering angle side of the *BETA* detector in order to minimize the background from the target and the beam line (see Fig 14).

Drastic shielding of the phototubes in this configuration will be possible. This design is different from the preliminary proposal design which considered instead 5" photomultipliers and had the photomultipliers mounted symmetrically on each side of the Čerenkov tank. Glass mirrors are preferred over plastic for their long term stability, they should maintain their curvature without creep and are not susceptible to crazing.

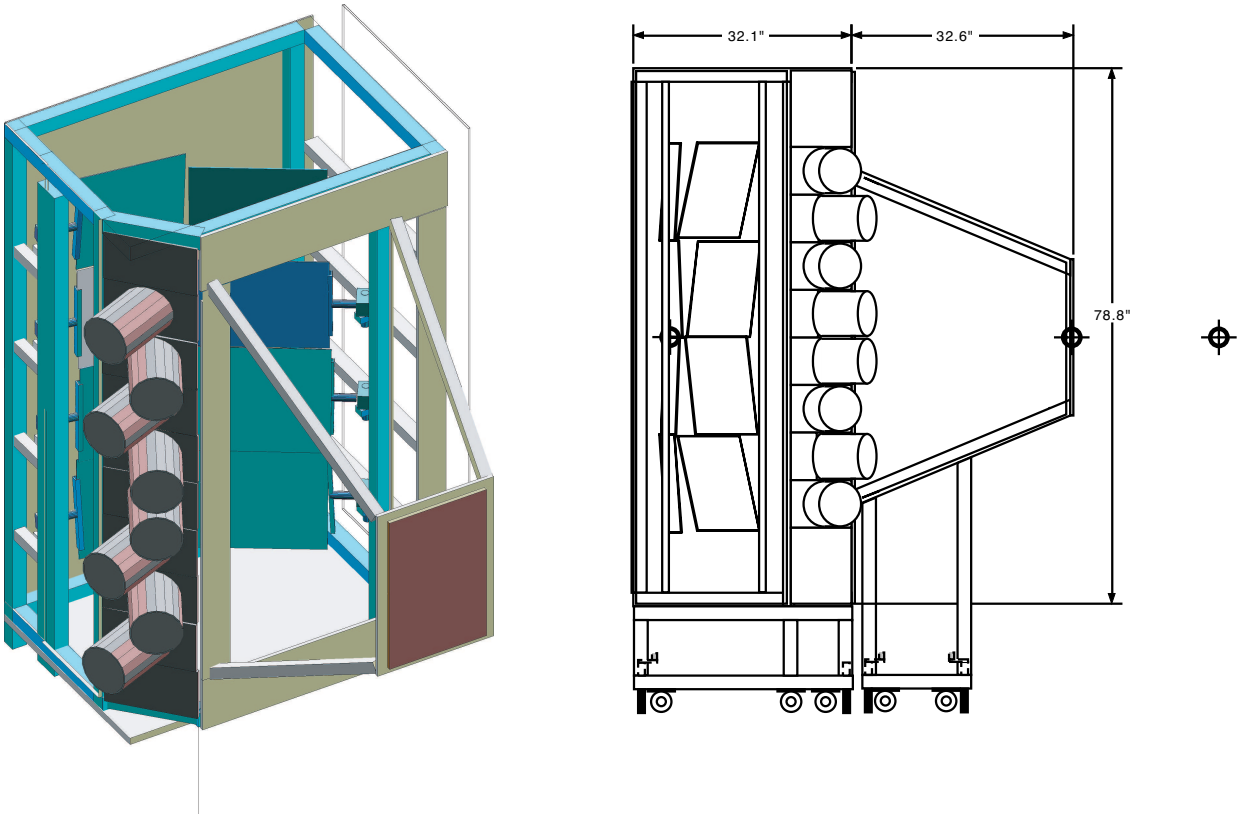

Figure 14: Left: three dimensional open view of the Čerenkov counter with its mirrors and phototubes. Right: open side view of the counter with its wheeled base. By sliding the front part of the tank, access to the mirrors is possible even when the BigCal detector and hodoscopes are in place.

To a good approximation, the mirrors have been designed for point-to-point focusing from the target cell to the photomultiplier photocathodes. This permits the two towers of mirrors to be optimally aligned with a small, bright light bulb located at the same target-mirror distance. This geometry also permits good rejection of stray light from scintillation and low energy δ rays (which are preferentially emitted at angles several times larger than the Čerenkov cone).

The coating of the mirrors is aluminum with a passivating and UV-extending layer of MgF_2. The reflectivity of the mirrors will be measured at CERN. We also plan to test the performance of these mirrors at delivery using a prototype tank which we have built and used in a parasitic mode in Hall C (see Fig. 15). These tests will be performed using a radioactive β source to generate electrons of few MeV and a thin quartz rod to generate Čerenkov photons in a broad spectrum of wavelengths starting in the UV regime. We also plan to ask for dedicated time in Hall C to test the full tank in a background environment similar to that of the real experiment.

Number of photoelectrons for the N_2 gas Čerenkov

Figure 15: A prototype gas Čerenkov counter tank built at Temple and used in parasitic tests in Hall C during 2005. It will be used to test the reflectivity of the mirrors when they are received from the manufacturer.

The number of Čerenkov photons emitted per cm per nm for N_2 gas at 20° C assuming a constant index of refraction n (= 1.000279) is

$$\frac{dN}{d\lambda} = \frac{2\pi z^2 \alpha}{\lambda^2}(1 - \frac{1}{\beta^2 n^2}).$$

Using a conservative lower cutoff of 200 nm, one estimates the number of photoelectrons per cm of gas traversed. For our design radiator gas thickness of 125 cm, assuming a mirror reflectivity of 90% and only 90% transmission through the gas-window interface due to Fresnel reflection, we can expect 20 photoelectrons when quartz windows are used. The photomultiplier tubes will be hermetically isolated from the often helium-rich environment near the target platform.

Pion rejection

At about $T_\pi = 0.5$ GeV, it becomes possible for a pion to scatter an electron above Čerenkov threshold, however the probability does not reach 0.01% until about $T_\pi = 0.75$ GeV. For a large range of pion energies, an N_2 radiator meets our requirement for 1000:1 charged pion rejection. Low energy, relatively large angle δ rays dominate the knock-on probability. These events produce few photoelectrons because they are barely above Čerenkov threshold. A tight, baffled focusing arrangement for the Čerenkov photons, combined with an aggressive electron definition cut (3-5 photoelectrons) will improve our pion rejection further. However, 1000:1 rejection is adequate for SANE.

A similar calculation was done for proton knock-ons. The knock-on probability for protons is negligible. It is harder for the much more massive proton to transfer enough energy to an electron to cross a Čerenkov threshold of about 21 MeV.

An alternative radiator gas

While nitrogen gas appears to be a near-optimal radiator for our application, it does have a weak scintillation yield which is relatively larger than other common radiator gases. This is not normally a problem since the emission is isotropic; the effects of scintillation are further reduced by the tight mirror focus, baffling, and black-painted walls. However, in the presence of very large charged particle backgrounds, this small scintillation yield can produce significant DC background in the gas Čerenkov signal [48].

We do not believe our charged particle backgrounds will be pathological. For the particles coming from the target, the rate of the high energy ones can be estimated and the low energy ones are cut off below 180 MeV/c due to the target magnetic field. For background originating

Figure 16: Left: 3D view of the photomultiplier holder and pointing alignment mechanism.

downstream of the target, there will be nothing but a Helium bag to intercept the spray of particles coming from the target. A $\geq$ 2" lead wall will shield BETA from this potential source of background. Nevertheless, the N_2 radiator gas could be replaced with CO_2 gas in a few hours without the need to realign the mirrors. This change would reduce scintillation and increase the number of photoelectrons, but worsen pion rejection.

Construction Status

Many elements of the Cherenkov counter have been completed or are near completion. The fabrication of the photomultipliers support systems which includes housing, holders and mu-metal shields has been completed (see Fig. 16 for the 8 photomultipliers support system). The mirrors mounts and their alignment system (translation and rotation) have been purchased and assembled, there are shown in Fig. 17. The mirrors glass blanks have been fabricated and are being shipped to CERN for aluminum and magnesium fluoride coating. Given the CERN coating facility schedule an agreed upon date of completion for the coating and measurement of the reflectivity has been given to us as March 01, 2007. We have also purchased nine (eight plus one spare) 3" quartz windows Photonis photomultipliers with including the bases.

The overall tank structure of the Cherenkov was fabricated at Alpha tools in New Jersey and its reception is imminent. As soon as it is received all necessary parts to assemble it are ready. Tedlar

windows and all gaskets have been prepared and pressure tested, the pressure control system has been built and tested too.

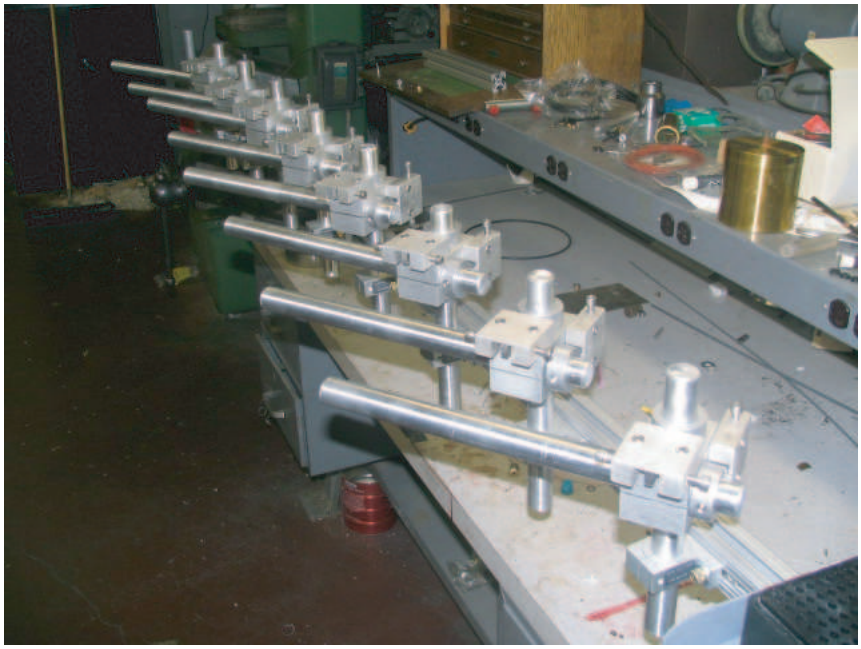

Figure 17: Eight mirror mounts

The readout electronics will consists of 8 channels VME ADCs and TDCs integrated to the Hall C data acquisition system. We are also considering the use of flash ADCs[1] to handle pileup events if they become dominant at the projected luminosity. The segmentation of the Čherenkov detector in eight sectors allows us to form geometrically correlated triggers between the hodoscopes and the Čherenkov counter. Due to the high average number of photoelectrons for good electrons the threshold on each sector will be set high (greater than five photoelectrons) to reject noise and scintillation without compromising the electron detection efficiency.

Our tentative plan is to test a fully equipped counter for intrinsic performance and background handling during the $GEp - III$ experiment scheduled to run in 2007 or separately with some dedicated beam time. We are working on coordinating the platform construction for the test and the experiment.

8 The Lucite Cerenkov Hodoscope

The Lucite Cerenkov hodoscope will be located between the Cherenkov and the BigCal calorimeter, at 240 cm from the target. The distance between the Lucite and BigCal is 80 cm. The purpose of the hodoscope is: 1) to detect charged particles above the threshold (primarily electrons and pions) with high efficiency; 2) to assist in providing a high level of $\pi^{\pm}$ rejection (1000:1) for the case of electron trigger; 3) to provide useful position resolution at a reasonable cost; and 4) to be insensitive to the background particles coming from outside of the target chamber.

[1]Plash ADC's being built by Jefferson Lab's Electronics Group, which are expected to be in production by October 2007

The refractive index for Lucite is n = 1.49. The threshold velocity for Cerenkov radiation inside the Lucite is $\beta = 0.67$. The bars of the hodoscope will be wrapped in black paper, without a reflecting layer. Therefore, the propagation of light to the PMTs would be through total internal reflection (TIR) only. The critical angle inside the Lucite is: $\theta_{TIR} = 42.2^o$, which implies that only photons with an angle of incidence larger than $\theta_{TIR} = 42.2^o$ would be detected. This condition restricts detection of particles with $\beta < 0.91$ as well as those with an impact angle other than $(90\pm1)^\circ$ with respect to the surface plane. The Cerenkov radiation angle is $\theta_C = 42.5^o$. Because there are no randomly reflected photons, the timing distribution of the detected light is narrow, and one can use the timing information for reconstruction of the coordinate of impact.

The Monte-Carlo simulation of the Cerenkov bar revealed a spatial resolution of $\sigma = 1.7$ cm for particles with impact angle near 90°, which can be quite adequate for the experiment (see figure 18).

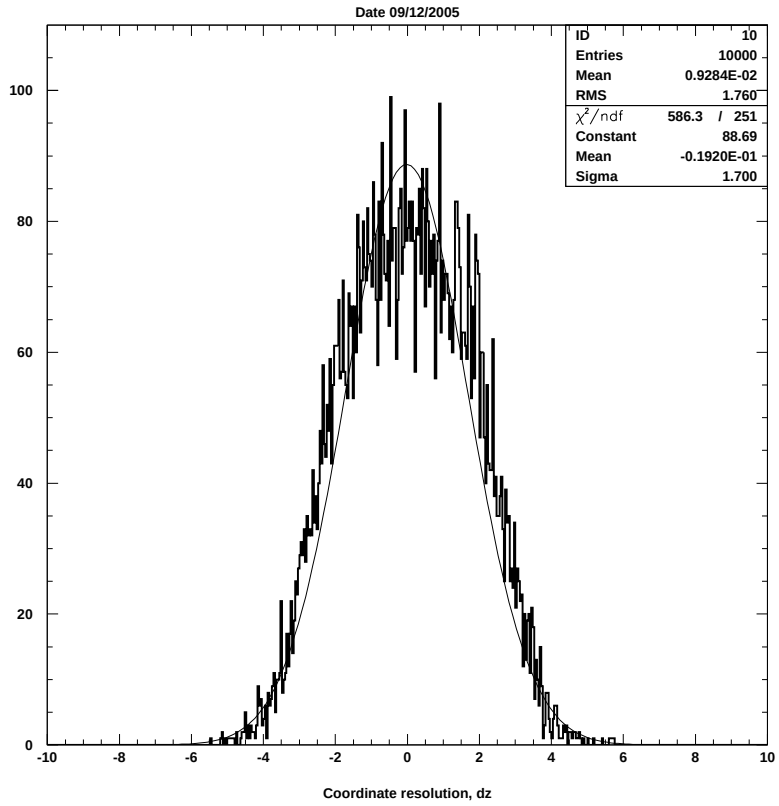

Figure 18: Monte-Carlo: Coordinate distribution of detected particles, reconstructed from timing information

Using the position information in the hodoscope ($\sigma < 1.7$ cm) and in the calorimeter ($(\sigma = \frac{6\text{mm}}{\sqrt{E(\text{GeV})}}$) one can trace back the particles to the target. The vertex resolution at the target will be $\sigma < 5$ cm, and the angular resolution, $\sigma_\theta < 0.8^o$. The restriction on the angles of detected particles will help eliminate the background coming from outside of the target cell. The schematic view of the hodoscope is presented in figure 19. The hodoscope consists of two planes: 32 horizontal and 16 vertical bars. The width of each bar is 6 cm.

Hodoscope Prototyping and tests with cosmic rays

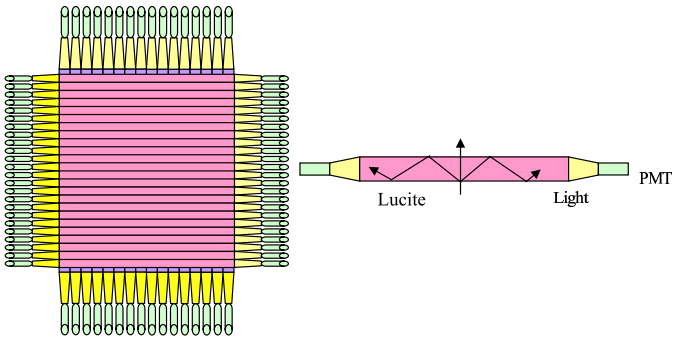

Figure 19: Lucite Cerenkov Hodoscope.

We have constructed a prototype bar and conducted tests with cosmic rays at the Nuclear Lab at NC A&T State University. The goal of this test was threefold: 1) to measure the coordinate resolution 2) to study the dependence of the impact angle on the coordinate resolution; and 3) to measure the number of photoelectrons in the PMT from the Cerenkov radiation. The experimental setup is presented in figure 20. The prototype bar size is $3 \times 6 \times 80$ cm^3 with a PMT mounted on each side (PMT_1 and PMT_2). The coincidence signal from the two scintillating detectors (Det_1 and Det_2) of size 10×10 cm^2 and placed underneath the bar was used as a trigger. Two lead bricks with a total thickness of 10 cm were used to select muons with $\beta > 0.92$. TDC and ADC information for all detectors were recorded.

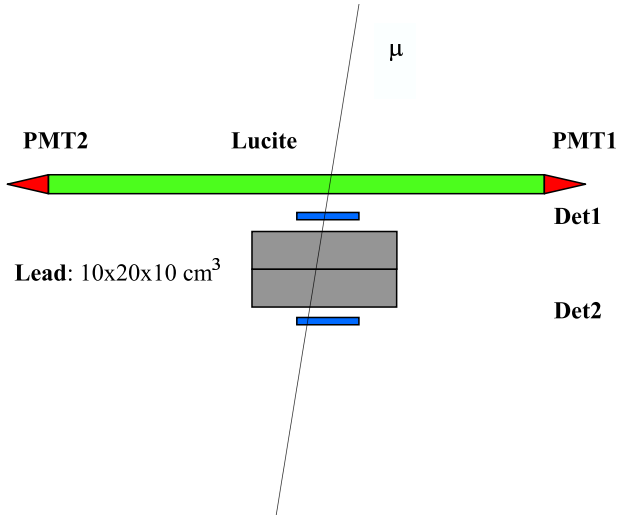

Figure 20: Detector setup for the prototype test with cosmic muons.

Off-line data analysis is fairly simple and consists of imposing a TDC cut which filters the events within ±2 ns around the peak value. A second cut on the ADC values restricts the angular distribution of the impact angle to roughly $(90 \pm 1)^\circ$. By doing so we can ensure that we have a TIR angle of 42.2° for detected Cerenkov photons. The results of the analysis are presented in figures 21 - 23.

Results and discussion

Results of the muon test are as follows:

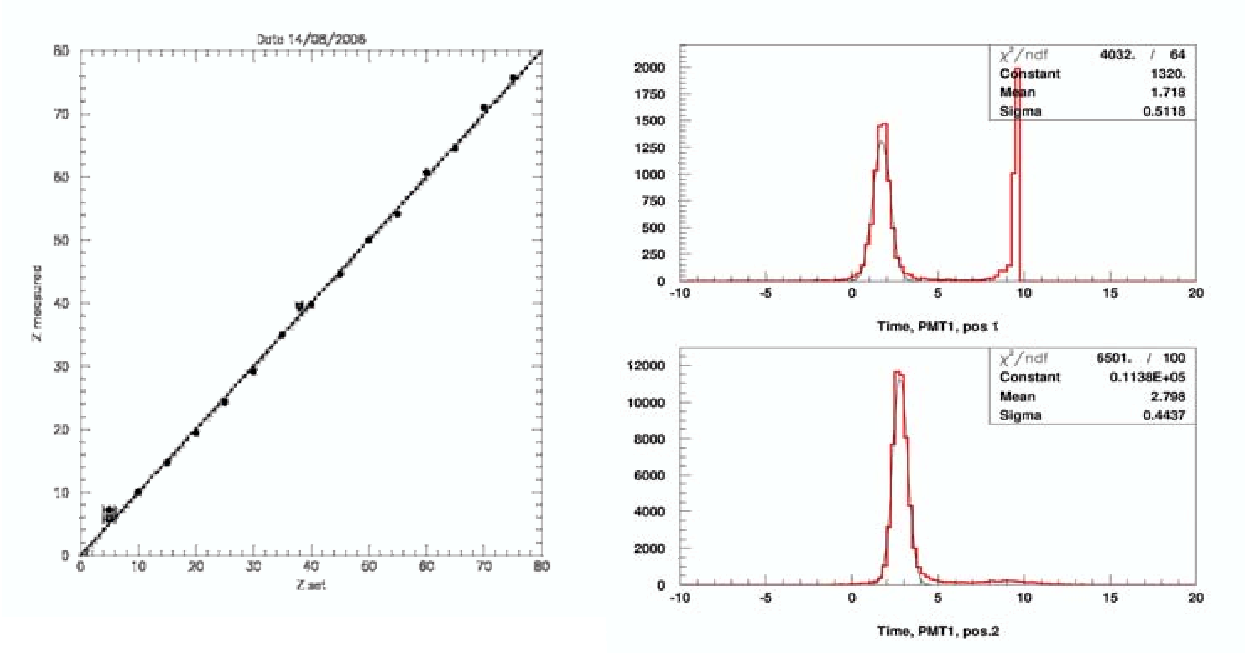

Figure 21: Left: reconstructed coordinates vs. measured; right: time distribution before (top) and after (bottom) cutting the bar's edges at 45^o

1. Coordinate resolution. By moving the prototype detector over the telescope of scintillators with a step of 5 cm, one can determine the dependence of the coordinate resolution on the position of impact. The reconstructed position (mean value of the distribution) is plotted vs. the measured position in fig. 21 (left). Two points, one at the center of the plot and the other at the left edge, were measured with 10^o inclination of the bar over the telescope. As one can see, the reconstructed value deviates from the measured one by a couple of centimeters. Reconstructed values at the edges of the detector don't fit exactly the measurements. The worst accuracy of reconstruction for a single event is about ± 3 cm at the edges, while at the center it is much more precise: ± 0.4 cm.

2. Reflection from the bar end surfaces: We found high level of reflection from the ends of the bar, as one can see on fig. 21 (right, top) and fig. 22 (left, top and bottom). The time distribution of the detected light in PMT1 is plotted in fig. 21 (right, top and bottom). On the top figure one can notice a second peak corresponding to the photons reflected from the PMT2-side bar end. The reconstructed impact coordinate distribution (fig. 22 left, top) and distribution of the reconstructed total length (fig. 22 left, bottom) contain two peaks. One is related to the impact coordinate ($< x > = 25$ cm) and total length ($< L > = 80$ cm, which is the total length of the bar). The second peak corresponds to the reflection from the interface ($< x > = 80$ cm, the coordinate of the opposite edge of the detector) and double length of the detector (160 cm). In order to reduce reflections from the interfaces, we have cut both edges at 45^o. With this cut, the propagated light would exit the bar perpendicular to the interface (since the propagation angle is 42-43 degrees) and the reflection would be dramatically reduced. The distribution on the right graphs of fig. 21 and two distributions on the right of fig. 22 demonstrate the effect of the cut: the reflection vanishes almost completely.

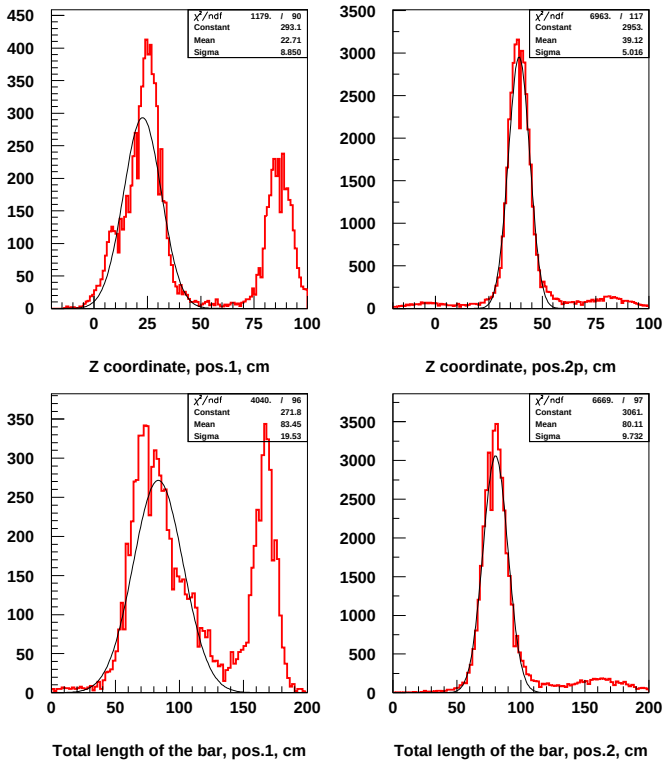

Figure 22: Left column: reconstructed coordinate distribution and the total length of the bar; right column: the same after cutting the edges at 45^o.

3. Number of photoelectrons: The ADC spectrum of PMT1 is plotted in fig. 23 before and after the 45° cut. The distributions in black color (narrow, tall peaks) correspond to the case without TDC restriction on the PMT1 time, while in blue (broader peaks) the distribution with narrow time cut (t < 3.5 ns on the plot in the fig. 21, right). Most likely, photons with small ADC values are those which were reflected from the interface of the opposite edge. The 45^o cut reveals that the peak from Cerenkov photons is at about 600 channels of ADC. Hence, reflections decrease the number of photoelectrons a few times. From the distribution on the right, which is an ADC distribution from the LED light, showing the number of the ADC for a single photoelectron, which is about 60 channels. We conclude that the number of photoelectrons detected by one PMT from the Cerenkov radiation of fast particles (β >0.91) is equal to 10 in a 3 cm thick Lucite bar.

To maximize the amount of light collected at the phototubes we are investigating two approaches:

- curve the bars to preserve normal incidence over the entire angular acceptance. The manufacturer indicated this would be possible.

- attach light guides at the bar ends to improve the match between the bar cross section and the PMT face.

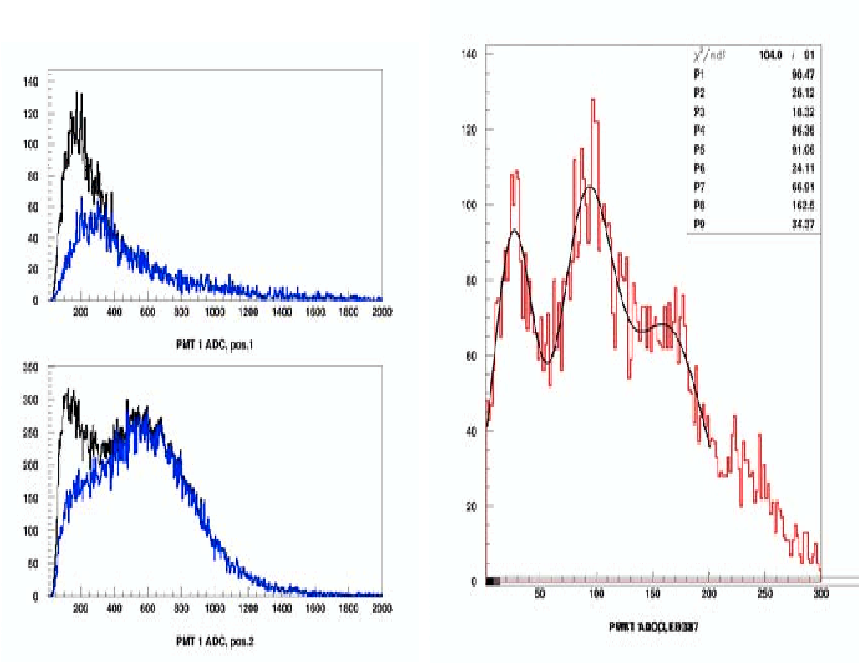

Figure 23: The ADC spectrum before (top left) and after (bottom left) cutting the edges; the broad peaks (blue) have a t< 3.5 ns cut. The ADC spectrum from the LED (right)

Beam test

Our goal is to perform two beam tests in Hall C during the spring of 2007, one of which will be done with dedicated beam time.

In the first test we plan to set up the prototype detector in Hall C and leave it exposed directly to particles from the target and to background radiation. Two narrow scintillators will be lined up with the target, at 40^o with respect to the beam to define the particle's direction. The test would be performed at a beam current of 1 μA. This would simulates the SANE conditions. The test would allow us to study the background conditions, test the coordinate resolution and study the detector efficiency at high singles rate.

The second beam test would be done in parasitic mode with the experiment E05-017. Two scenarios are possible: 1) set up the prototype detector in front of the calorimeter inside the HMS detector hut and 2) set up the detector right behind the SOS tracking chambers. This test would allow us to measure the efficiency and coordinate resolution of the prototype detector and check their dependence on the momentum, on impact angles and on the position of the incoming particles. We have consulted with the E05-017 spokespersons and the Hall management about these test plans.

Final design and construction

The results of the muon tests and the two beam tests would help us finalize the design of the detector. We anticipate to achieve a final design by late spring of 2007. The construction of the detector will then starts in summer-fall of 2007.

Hall C has purchased 32 PMT's and bases. The remainder will be purchased with NC A&T State University funds.

9 Forward Tracking Hodoscope

The Forward Tracking Hodoscope is the first element of the BETA detector package. The main purpose of this $X-Y$ hodoscope detector is to provide redundant and efficient electron detection with limited tracking to suppress background. The detector will provide improved target position resolution (to better than 0.5 cm) in addition to its ability to reject non-target related backgrounds. An additional goal for the hodoscope is the partial ability to determine the sign of low momentum charged particles to discriminate positrons from electrons. This will allow the ability to measure positron asymmetry. Positron asymmetry has been well measured for longitudinal polarization in Hall B (EG1b program [16]) but only transverse measurements are at 29 GeV from SLAC with limited statistics. Ability to detect low momentum positrons in this detector will allow measurements of positron asymmetry for transverse polarization of the target. In addition, this will enable us to partially reduce positron contamination of the electron sample and also reject low momentum π^+ events.

In order to be able to determine the sign of low momentum charged particles and to reduce contributions from knock-ons to the gas Čerenkov detector background, the hodoscope needs to be placed close to the target. Additionally, the detector needs to be as thin as possible. Simulation studies of vertical excursion (Δy) of a 1 GeV/c momentum particle with the target magnetic field turned on compared to the trajectory with the field off to reach the same position at the calorimeter were performed to study the optimum location of the detector position. The results are shown in figure 24. For both positively and negatively charged particles, the vertical excursions are smallest at a scattering angle of $\theta = 33^\circ$ and largest at $\theta = 47^\circ$. The sensitivity for the determination of particle charge sign is maximal at about 20 cm from the target. With the target outer vacuum can radius at $\sim$ 48 cm, placement of the hodoscope at the desirable distance of 20 cm is not possible. The closest to the target one can put the hodoscope is at 50 cm, directly upstream of the gas Čerenkov detector, where the target magnetic field is $\sim$ 4 kG. A vertical position resolution of $\sigma_y \sim 2-3$ mm is necessary to be able to determine particle charge sign.

The size of the hodoscope placed at 50 cm from the target needs to be 40 cm (vertical) $\times$ 22 cm (horizontal) to be able to cover the geometrical solid angle of 219 msr of the BETA calorimeter. Also, the location of the hodoscope in front of the gas Čerenkov detector determines its maximum thickness by the need to minimize secondary particle production. In addition, to achieve the required vertical position resolution and to reduce the contributions from knock-ons, the hodoscope needs to be of high granularity and relatively thin in depth. The cross sectional area of individual counters in both $x-y$ dimensions needs to be about 3×3 mm^2. This will provide σ_{x-y} of about 3.0 mm/$\sqrt{12} \sim 0.9$ mm. Additionally, the hodoscope will consist of two Y-planes measuring vertical position, with 1.5 mm offset, for redundancy, and one X-plane measuring horizontal position of the charged particles. Table 4 gives the dimensions of the individual counters of the hodoscope and the total number of counters needed for the three $X-Y$ planes.

Table 4: Dimensions of individual counters of the Forward Tracking Hodoscope.

Type	Thickness (cm)	Horizontal Dimension (cm)	Vertical Dimension (cm)	Quantity
X	0.3	0.3	40.0	73 bars
Y	0.3	22.0	0.3	133×2 bars
			Total:	339 bars

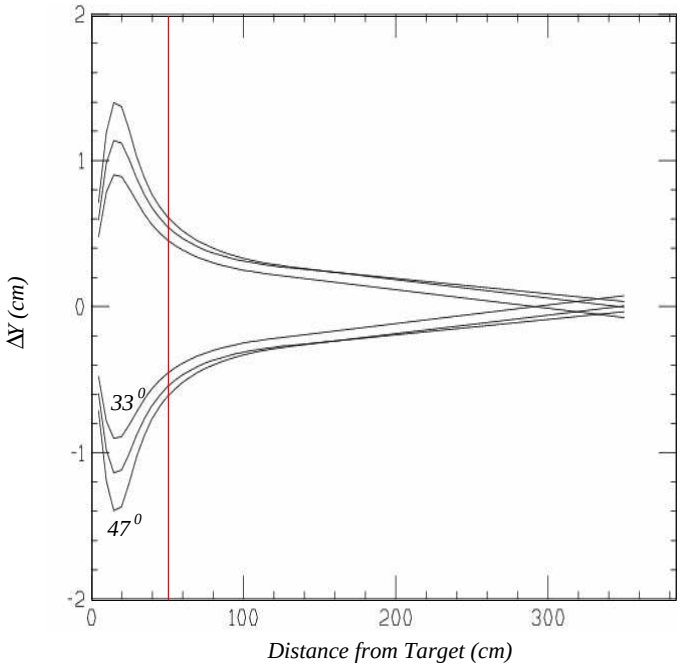

Figure 24: Plot shows typical difference in vertical excursion (Δy) versus distance from the target of $P = 1$ GeV/c particle withe the target magnetic field turned on and off for scattering angles between $\theta = 33^\circ$ and 47° for positively and negatively charged particles. The vertical line (red) shows separation at a distance of 50 cm from target.

The initial design of the hodoscope considered a solid Čerenkov detector made of quartz with an index of refraction $n = 1.47$. Quartz was the material of choice due to its insensitivity to charge particles below the β threshold as well as to low energy γ background and to neutrons. A sample quartz (Spectrosil 2000) bar (with dimensions $35 \times 0.5 \times 0.3$ cm^3) was obtained from Saint-Gobain Quartz to study the photoelectron yield and attenuation of Čerenkov light along the bar length. Tests of the quartz bar with cosmic ray muons showed that even though there was no noticeable light attenuation along the length of the bar, the average number of photoelectrons was very low, $\sim 2-3$ p.e. per MeV. This low photoelectron yield will be quite inadequate for obtaining a good signal for the purpose of track reconstruction of the charged particles.

In the current design, the hodoscope is being constructed with scintillators (Bicron BC-408 from Saint-Gobain Crystals). Since the detector will be located at 50 cm from the target, where the magnetic field is ~ 4 kG, ordinary photomultiplier tubes coupled directly to the scintillators will be inoperable for detecting the light output. Instead, scintillation light collection will be performed by blue-green wavelength shifting fibers (Bicron BCF-92 fibers, 1.2 mm diameter $\times$ 2.5 m long) attached directly onto the surface and along the length of individual scintillators. The light output from the fibers will then be detected by 64-channel multianode photomultiplier tubes (Hamamatsu H7546B). Such a scheme of scintillator-wavelength shifting fiber combination for the light output readout system has been successfully employed in other projects, for example, the TESLA project at DESY [49], and the MINERνA project at Fermilab [50]. Based on test results of the forward calorimetry in the TESLA project, where the individual scintillator geometry is very similar to the SANE hodoscope, the average number of photoelectrons is expected to be $\sim 10-15$ p.e. per MeV for SANE. The event rates for individual scintillators is expected to be ~ 10 kHz from background

(neutrons, pions, protons, and electrons) rate studies done in Hall C during the G_E^n experiment (E93-026) [51] for comparable target luminosity as proposed for SANE. Also, the total radiation length of scintillator for the three planes of the hodoscope is $\sim 2.1\%$ which will not deteriorate the energy resolution of the BETA calorimeter in any significant way.

The hodoscope is not expected to be part of the event trigger for SANE. The readout electronics for each anode of the multianode photomultiplier tubes attached to individual counters of the hodoscope will be through a discriminator signal going into a TDC. The level of cross-talk between the anodes of the Hamamatsu H7546B PMT unit is typically 2% and this will not affect the physics asymmetry results of the experiment. The required number of discriminators and TDC modules for the detector are already on-hand in Hall C.

Currently, all scintillator bars, wavelength shifting fibers, and the multianode photomultiplier tubes to build the hodoscope have been ordered and delivery of all items is expected by early January, 2007. Enough scintillator bars, fibers, and photomultiplier tubes to build a prototype 64 channel Y-plane will be on-hand by early December, 2006. Construction of the prototype plane is in progress (some of the hardware are already on-hand) for possible beam test during early Spring, 2007.

10 Polarized Target Outer Vacuum Can (OVC) and Related Target Items

Window design

The overall dimensions of the OVC for SANE are quite similar to the one used in Gen01/RSS experiment. The inner radius is 45.6 cm, and the wall thickness is 0.935 in. The OVC window design was done and submitted to the JLab Engineers in May 2006. Since then, a few minor changes in window locations and dimensions were made. Because of BigCal's large acceptances (218cm(H)x120cm(W)), each BETA window needs to be quite large. Because this vacuum chamber will be used in three polarized-target experiments in Hall C (SANE, Semi-SANE, and Wide-Angle Compton Experiment (WACS)), the physics requirements from the three experiments were considered in the window design [53].

Figure 25 shows the angle locations of the window. The windows for SANE are shown in red (dark grey). The details of the OVC design as of Aug. 2006 are given in [53]. Because the scattered electrons are deflected due to the 5-T magnetic field at the target, we ran a simple Monte-Carlo simulation program [54] to estimate the *minimum* window size by looking at the distribution of particles when they go through an OVC window location at R=46 cm. The minimum window height for SANE (for both parallel and perpendicular configurations) is estimated to be 34 cm. Because the BigCal during WACS will be located at 2.5 m from the center of the target (while it is at 3.5 m during SANE and Semi-SANE), the height of the WACS window (shown in green (light grey) in the figure) needs to be at least 44 cm. All of the four big windows therefore have the same height of 46.0 cm, and are made as wide as possible. Although those windows are rectangular in shape, each corner of the window is rounded with the radius of curvature being 2.0". The largest window we have is the SANE perpendicular window (46 cm(H)x47.7 cm(W)). The OVC windows are made of 2024-T3 Aluminum. The window thickness has not been determined yet but we are assuming that it is 0.019" thick.

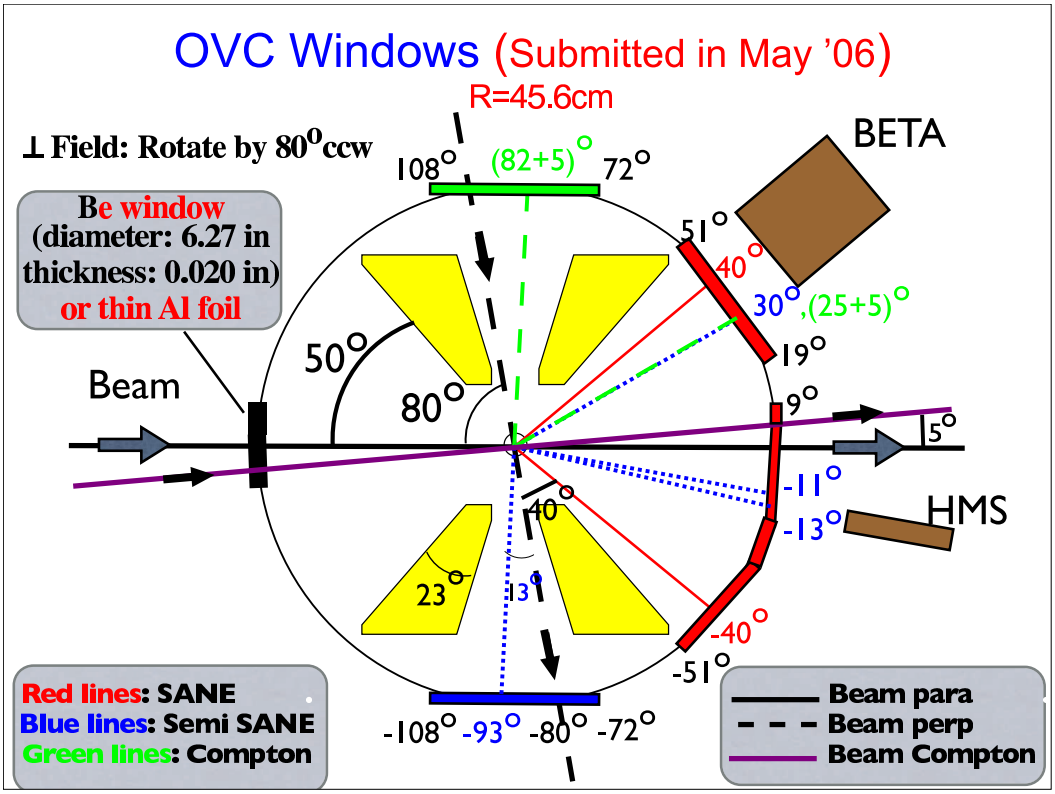

Figure 25: OVC Window location (top view). SANE windows are shown in red (dark grey). The window for SANE parallel (perpendicular) running is located from -51^0 to $+9^0$ (from $+19^0$ to $+51^0$). The red lines (thin solid) indicate the central angles of the BETA detector during SANE.

Beam Entrance Window for SANE Parallel

As shown in Figure 25, the beam entrance window for SANE Parallel is larger than normal because the WACS collaboration is planning to rotate the can by 5° clockwise for their measurement [55]. According to the current design, this beam window is made of Beryllium of 6.27 in diameter that JLab owns, but there is a possibility of using other material such as aluminum instead.

Nitrogen Shield

The Nitrogen Shield, which will be installed inside the OVC, is also designed. The window locations and dimensions are quite similar to the OVC design. The inner radius of the shield is 41.5 cm and its thickness is 1/4". We will mount around each rectangular window a frame 1/8" thick which stands off the nitrogen shield. Either thin aluminum foil or super insulation will be attached to the frame. Vacuum will be pumped through the 3 mm gap between the nitrogen shield and the frame. Fig. 26 is an engineering picture of the vacuum chamber with OVC windows, nitrogen shield, and window clamps.

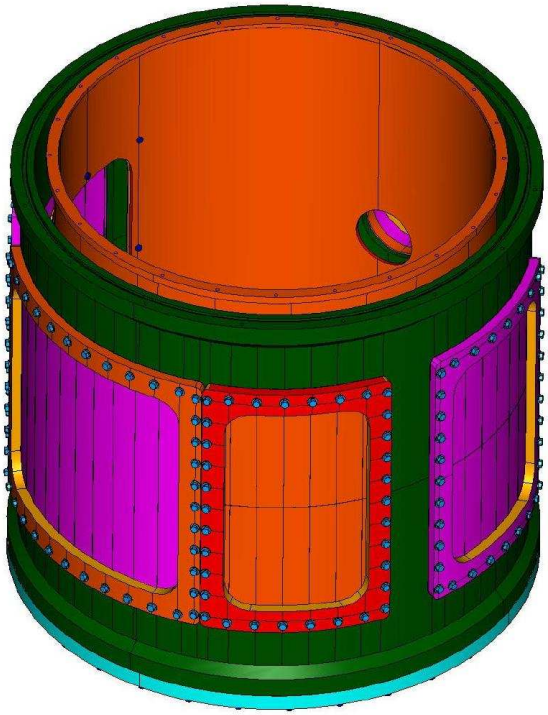

Figure 26: An Engineering picture of the vacuum can. (prepared by B. Metzger). The vacuum can is shown in green (dark grey), and the nitrogen shield is installed inside the OVC, shown in orange (light grey). We assumed that the radius of curvature at each window corner is 2.0".

Status and Engineering Design

The JLab engineers have performed finite-element calculations assuming that the window thickness is 0.019". According to their calculations, this thickness may be insufficient, given the current windows shapes. The engineers have been working on design modifications to keep the windows as thin as safely possible. They are also planning to perform tests using the $GEp-III$ window fixture (112 cm x 43 cm), which is much larger than our largest window, in order to validate their finite-element analysis. The tests are on hold pending the delayed arrival of the fixture.

10.1 Target materials

SANE plans to use ordinary frozen NH_3 as the target material. The UVa polarized target group has purchased a substantial amount ($\sim$ 200 g) of ammonia, to meet the needs of the approved JLab experiments that will use the solid polarized target. Freezing of the material in preparation for its irradiation is ongoing at UVa. Irradiating ammonia creates the necessary centers to polarized the material by the dynamic nuclear polarization (DNP) technique. The irradiations will be carried at NIST in 2007.

11 Auxiliary systems

The intense 5 T target magnetic field strongly deflects both the incident beam (when aligned at 80°) and the scattered electrons. The scattered electron deflections are symmetrical about the horizontal mid-plane for $A_{\|}$ and near-$A_{\perp}$, because of the 40° central alignment of BETA. The deflection of the beam by the field before scattering must be corrected by the chicane, so the beam is horizontal at nominal beam height at the center of the target. The target $\int Bdl = 1.52$ T-m at 80° is compensated by the BE and BZ1 magnets. Entrance and exit angles for those magnets are given in Table 5 for the two beam energies for which 80° data will be taken, along with vertical deflections at relevant points. The currents needed to drive BE and BZ1 to the required fields are within the magnet power supplies specifications.

E GeV	Angle exit BE to BZ1	BZ1 bend	BZ1 deflection m	Target angle	Int Bdl BZ1 T-m	Int Bdl BE T-m	Int Bdl Target T-m
4.634	0.897	3.716	0.16	2.819	1.003	0.512	1.521
5.792	0.718	2.974	0.131	2.256	1.003	0.519	1.521

Table 5: Table of approximate corrector chicane settings for SANE. Angles in degrees.

The concentrated CEBAF beam needs to be distributed uniformly over the polarized target cross section to avoid rapid depolarization due to heating and radiation damage. This is done by the Hall C slow raster system, which will be operated in a 2 cm maximum diameter spiral pattern, as in previous experiments [56, 20]. The 2x2 mm Hall C fast raster is superimposed on the slow raster pattern.

Since the HMS is a software spectrometer that relies on knowledge of the nominal beam position at the target for its reconstruction algorithms, the target Secondary Emissions beam position monitor (SEM TBPM) will be installed upstream of the target as in previous experiments [56, 20]. The SEM records the position of the beam 30 times per second with a resolution of 1 mm. The SEM information is saved in the event record and used for the scattered trajectory reconstruction. The SEM was sent to the University of Basel, where it was built, to be refurbished in preparation for SANE, and it is ready to be returned to JLab installation.

12 Collaboration Status

After Dr. Glen Warren, who was one of the two original SANE co-spokesmen left the field of medium energy electronuclear physics, Prof. Zein-Eddine Meziani (Temple U.) and Prof. Seonho Choi (Seoul U.) accepted the invitation to become co-spokesmen along with Oscar Rondon.

Since our first collaboration meeting at JLab in November 2003, we have organized a series of trimestral meetings, at JLab and the University of Virginia (May 2006). The 12th. meeting in the series took place this past December 1st., at JLab, attended by close to 30 collaborators. The agenda of topics discussed at the meeting is shown below. It is illustrative of the level of

commitment of the collaboration's member institutions:

Welcome	*O. Rondon (U. Va)*
Hall C Schedule Update	*S. Wood (Hall C)*
Report on Gas Cherenkov Status	*Z − E. Meziani (Temple)*
Update on BigCal	*M. Jones (Hall C)*
Report on Gain Monitor	*E. Frlez (U. Va)*
Report on Front Tracking Hodoscope	*M. Khandaker (NSU)*
Report on Lucite Hodoscope	*A. Ahmidouch (NC A & T SU)*
Status of Polarized Target Vacuum Can	*S. Tajima (U. Va)*
BETA's GEANT simulations	*J. Maxwell (U. Va)*
BigCal energy calibration	*G. Huber (U. Regina)*
Update at PAC31	*O. Rondon*

Copies of the reports presented at the meetings by the collaboration and many other useful documents are posted at SANE's Web site `http://www.jlab.org/ rondon/ sane`. The reports presented at the past three Hall C January Users meetings are posted there as well.

The collaboration membership has grown substantially since the PAC approval, now consisting of 15 institutions and over 50 physicists, of which at least two are expected to write dissertations on SANE.

13 Beam Request

We have submitted a beam request for consideration at the recent beam scheduling meeting. We reiterate our request to be scheduled for beam in Hall C at the earliest opportunity consistent with the constraints of previously scheduled experiments, available beam energy $\geq$ 5.7 GeV, and the requirements of a large installation experiment, as detailed in the documents on file.

For reference, we attach our preliminary run plan, based on the Hall C long range plan, which indicates the period February 19 to March 31st., 2008 as SANE installation, and data taking starting on April 1st., 2008 for 27 PAC days. The final run plan will reflect the actual schedule.

Start: 04/01/08
Finish: 05/25/08

SANE Run

Page #1

	Activity Name	Duration	Start	Finish
1	SANE Run	54	04/01/08	05/24/08
2	Commission/Calibration	5	04/01/08	04/05/08
3	Energy change 2 pass => 4 pass	1	04/06/08	04/06/08
4	4.6 GeV parallel	4	04/07/08	04/10/08
5	Target rotation 180° - 80°	1	04/11/08	04/11/08
6	Chicane alignment	0	04/11/08	04/11/08
7	4.6 GeV 80 deg.	10	04/12/08	04/21/08
8	Energy change 4 pass => 5 pass	1	04/22/08	04/22/08
9	Chicane alignment (if needed)	0	04/22/08	04/22/08
10	5.7 GeV 80 deg.	21	04/23/08	05/13/08
11	Target rotation 80° - 180°	1	05/14/08	05/14/08
12	Chicane alignment	0	05/14/08	05/14/08
13	5.7 GeV parallel	10	05/15/08	05/24/08

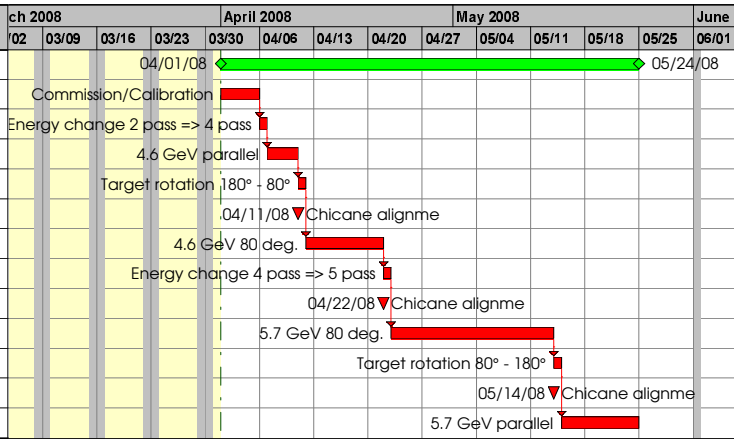

Table 6: Preliminary SANE run plan.

Considering the actual restrictions on availability of manpower (weekdays vs weekends, day shift vs swing shift, etc.) for major overhead operations such as alignments, target rotations, etc., the preliminary run plan's approximate distribution of running times based on the original proposal and PAC24 approved beam days is as follows:

Commissioning and calibration: 60 h - 5 calendar days
Parallel data at 4.6 GeV: $\leq$ 70 h - 4 calendar days
80° data at 4.6 GeV: 130 h - 10 calendar days
80° data at 5.7 GeV: 200 h - 21 calendar days
Parallel data at 5.7 GeV: 100 h - 10 calendar days

plus four calendar days exclusively for overhead. Emphasis is placed on the measurements at 80° degrees (31 calendar days vs 14 days for parallel). This distribution will of course be optimized dynamically during the run.

13.1 Installation Requirements

The installation requirements for SANE have been specified in the beam request documents. A summary is given below.

13.1.1 Target and beam line related

This experiment requires extensive support from the JLab. In addition to the installation of the polarized target, we will also require:

- installation of the Secondary Emission Monitor (SEM) (assistance to U. Basel physicist),
- beam line instrumentation workable down to 50 nA beam current,
- the two upstream chicane magnets,
- 1 cm maximum radius spiral slow raster and Hall C fast raster operational,
- downstream beam duct and He gas bag to transport beam to beam dumps. The duct and bag must accommodate both straight through beam to the standard Hall C dump and beam deflected by the target field during the near-$A_\perp$ data taking to a special in-hall dump.

These are the same requirements as for the $GEn-2001$ and RSS experiments that ran from Aug. 2001 through March 2002, so they present no special development for the laboratory.

13.1.2 BETA, HMS and shielding related

Although much of the work will be done by the collaboration, to assemble and operate BETA, SANE requires support for

- Design and construction of platform to support the gas Cherenkov, forward and Lucite hodoscopes, with room for maintenance access to the detectors. The platform will be located adjacent to the left of the target platform, upstream of BigCal's stand.
- Design and construction of support frames for the elements of the forward and Lucite hodoscopes.
- Annealing by exposure to intense UV light of expected radiation damage to BigCal's glass during $GEp-III$.

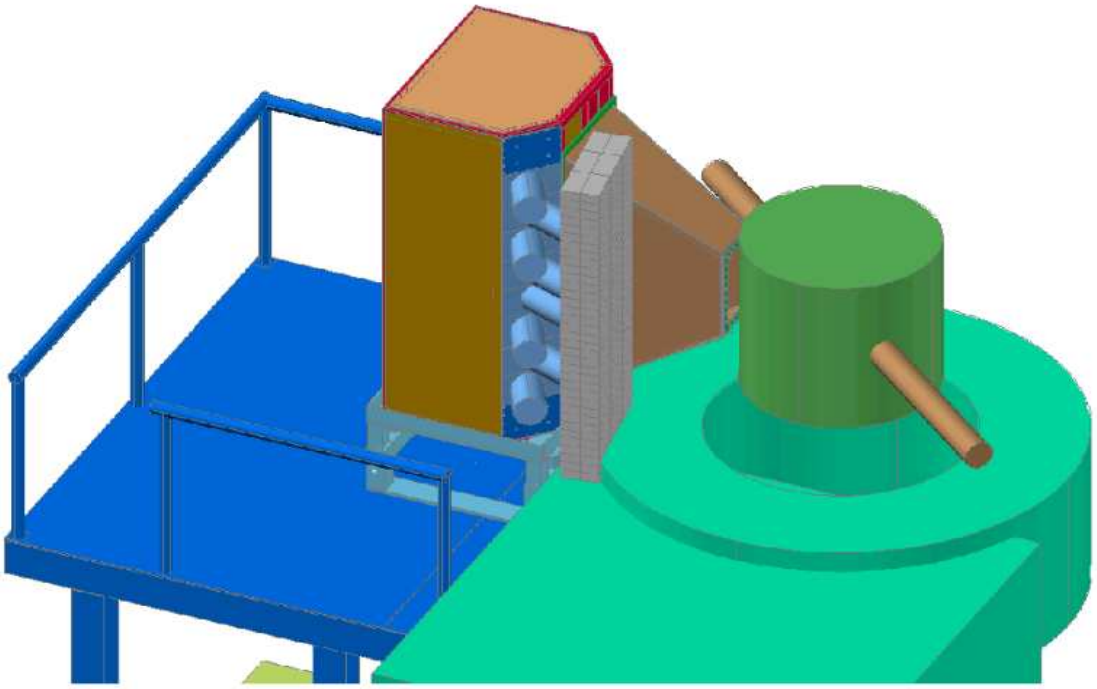

Figure 27: Artist view of Cherenkov on platform adjacent to polarized target. A wall of lead bricks shielding the photomultipliers is also shown.

- Removal of the focal plane polarimeter from HMS hut and re-installation of the Cherenkov.
- Stands or platforms to support lead brick shielding to protect BETA from beam line background, in a configuration similar to that used for the neutron detector [51] in the 1998 run of *GEn* [56].

References

[1] SLAC E80, M. J. Alguard *et al.*, Phys. Rev. Lett. **37**, 1261 (1976); **41**, 70 (1978).

[2] SLAC E130, G. Baum *et al.*, Phys. Rev. Lett. **51**, 1135 (1983).

[3] EMC, J. Ashman *et al.*, Nucl. Phys. **B328**, 1 (1989)

[4] SLAC E142, P. L. Anthony *et al.*, Phys. Rev. Lett. **71**, 959 (1993).

[5] SLAC E154, K. Abe *et al.*, Phys. Rev Lett. 79 (1997) 26.

[6] A. Airapetian *et al.*[HERMES Collaboration], hep-ex/0609039

[7] SLAC E143, K. Abe *et al.*, Phys. Rev. D **58**, 112003 (1998).

[8] SMC, B. Adeva *et al.*, Phys. Rev. D **58** 112001-1 (1998).

[9] SLAC E155, K. Abe *et al.*, Phys. Lett. **B463**, 339 (1999).

[10] P. L. Anthony *et al.*[E155 Collaboration], Phys. Lett. **B458**, 529 (1999).

[11] P. L. Anthony *et al.*[E155 Collaboration], Phys. Lett. **B553**, 18 (2003).

[12] A. Airapetian *et al.* [HERMES Collaboration], Phys. Rev. Lett. **92**, 012005 (2004)

[13] B. Adeva *et al.* [Spin Muon Collaboration], Phys. Lett. B **420**, 180 (1998)

[14] E. S. Ageev *et al.* [COMPASS Collaboration], Phys. Lett. B **633**, 25 (2006)

[15] A. Airapetian *et al.* [HERMES Collaboration], Phys. Rev. Lett. **84**, 2584 (2000)

[16] K. V. Dharmawardane *et al.* [CLAS Collaboration], Phys. Lett. B **641**, 11 (2006)

[17] X. Zheng *et al.* [Jefferson Lab Hall A Collaboration], Phys. Rev. Lett. **92**, 012004 (2004)

[18] R. Fatemi *et al.* [CLAS Collaboration], Phys. Rev. Lett. **91**, 222002 (2003)

[19] J. Yun *et al.* [CLAS Collaboration], Phys. Rev. C **67**, 055204 (2003)

[20] [RSS Collaboration], "Proton spin structure in the resonance region," arXiv:nucl-ex/0608003.

[21] N. Liyanage, AIP Conf. Proc. **747**, 118 (2005).

[22] X. Zheng *et al.* [Jefferson Lab Hall A Collaboration], Phys. Rev. C **70**, 065207 (2004)

[23] S. Wandzura and F. Wilczek, Phys. Lett. B172 (1977) 195.

[24] J. L. Cortes, B. Pire and J. P. Ralston, Z. Phys. C55 (1992) 409.

[25] R. L. Jaffe and Xiangdong Ji, Phys. Rev. **D 67** (1991) 552.

[26] X. Artru and M. Mekfi, Z. Phys. C **45**, 669 (1990).

[27] M. Göckeler *et al.*, Phys. Rev. D **72** 054507 (2005).

[28] E. Stein *et al.*, Phys. Lett. B **343**, 369 (1995).

[29] I. Balitsky *et al.*, Phys. Lett. B **242**, 245 (1990); B **318**, 648 (1993) (Erratum).

[30] B. Ehrensperger and A. Schäffer, Phys. Rev. D **52**, 2709 (1995).

[31] M. Stratmann, Z. Phys. C **60**, 763 (1993), and private communication for values at $Q^2 = 5$ $(\mathrm{GeV/c})^2$.

[32] H. Weigel, L. Gamberg and H. Reinhart, Phys. Rev. D **55**, 6910 (1997).

[33] M. Wakamatsu, Phys. Lett. B **487**, 118 (2000), and private communication.

[34] X. Ji, hep-ph/9510362.

[35] E. Stein, P. Gornicki, L. Mankiewicz and A. Schafer, Phys. Lett. B **353**, 107 (1995); E. V. Shuryak and A. I. Vainshtein, Nucl. Phys. B **201**, 141 (1982);
Philippe Grenier, *Etude des Fonctions de Structure en Spin du Nucleon: L'Experience E143 au SLAC*, Ph. D. Thesis, Saclay 1995, unpublished.

[36] G. Warren and O. Rondon, co-spokespersons, *SANE Spin Asymmetries on the Nucleon Experiment*, JLab Experiment 03-109.

[37] O. A. Rondon, M. Jones, spokespersons *Precision Measurement of the Nucleon Spin Structure Functions in the Region of the Nucleon Resonances*, JLab Experiment 01-006.

[38] K. Kramer *et al.*, Phys. Rev. Lett. **95**, 142002 (2005) [arXiv:nucl-ex/0506005].

[39] *Report to the Nuclear Science Advisory Committee*, submitted by the Subcommittee on Performance Measures, Nov.18, 2003,
`http://www.sc.doe.gov/np/nsac/docs/nsac_report_performance_measures.pdf`

[40] S. D. Bass, Rev. Mod. Phys. **77**, 1257 (2005)

[41] E. Brash, M. Jones, C. Perdrisat, V. Punjabi *Measurement of GEp/GMp to Q2=9 GeV2 via recoil polarization*, TJNAF E-04-108

[42] A.D. Martin, R.G. Roberts, W.J. Stirling and C R.S. Thorne, hep-ph/0110215

[43] The RadPhi Decay Experiment Home Page URL: `http://www.jlab. org/~ radphi/`, (Accessed on Oct. 16, 2006).

[44] B. B. Brabson *et al.*, Nucl. Instr. and Meth. **A332** (1993) 419.

[45] E. Frlež, *et al.*, Fizika B, 12, (2003) 97.

[46] Cyro Industries URL: `http://www.cyro.com/`, (Accessed on Oct. 16, 2007).

[47] Hamlet Mkrtchyan, Private Communication (2006).

[48] M. Buenerd, "Study of the Background in the E154 Data", April 22, 1996. Unpublished.

[49] Ralph Dollan, "*Investigation of a Crystal Calorimeter Technology with Longitudinal Segmentation*", Diplomat, Humbolt University at BERLIN, 1997.

[50] MINERνA Collaboration, Proposal for Fermilab Experiment E938, hep-ex[0405002]

[51] Oscar A. Rondon, "*Shielding in Expt. 93-026 - G_E^n*", JLab Expt. G_E^n Technical Note TN 99-06, 1999.

[52] Y. S. Tsai, Rev. Mod Phys. 46 (1974) 815

[53] S. Tajima. *Status of the Polarized Target Vacuum Can* (Slides presented at the SANE collaboration meeting on Aug.16, 2006.) http://www.jlab.org/~rondon/sane/mtg11/target_shige.pdf

[54] M. K. Jones. *Private communications*

[55] D. Day and B. Wojtsekhowski (E-05-101 Spokespersons) *Private communications*

[56] Donal Day, *The Charge Form Factor of the Neutron*, TJNAF E-93-026